JOURNAL OF PETROLOGY | VOLUME 39 | NUMBER 4 | PAGES 689–710 | 1998

Experimental Constraints on Himalayan Anatexis

ALBERTO E. PATIÑO DOUCE[1]* AND NIGEL HARRIS[2]

[1]DEPARTMENT OF GEOLOGY, UNIVERSITY OF GEORGIA, ATHENS, GA 30602, USA

[2]DEPARTMENT OF EARTH SCIENCES, THE OPEN UNIVERSITY, MILTON KEYNES MK7 6AA, UK

RECEIVED APRIL 28, 1997; REVISED TYPESCRIPT ACCEPTED NOVEMBER 20, 1997

We have melted metapelitic rocks from the High Himalayan Crystalline Sequence that are likely sources of leucogranite magmas. Starting materials were a muscovite schist and a tourmaline-bearing muscovite–biotite schist. Both are kyanite-zone rocks from the hanging wall of the Main Central Thrust. Experiments were conducted at 6, 8 and 10 kbar and 700–900°C, both without added H_2O (dehydration-melting) and with 1–4 wt % added H_2O. Dehydration-melting begins at 750–800°C, and produces melts that are virtually identical in composition to the Himalayan leucogranites. Adding H_2O lowers the solidus by promoting plagioclase + quartz melting. Melts produced from these starting materials at $T \leq 750°C$ by H_2O-fluxing are trondhjemitic, and different in composition from most Himalayan leucogranites. Leucogranite magmas in the Himalaya formed by dehydration-melting of metapelites during adiabatic decompression, at 6–8 kbar and 750–770°C. The dehydration-melting solidus for muscovite schist has a smaller dP/dT slope than that for biotite schist. In consequence, muscovite schist undergoes decompression-melting more readily than does biotite schist. The two solidi probably cross over at ~10 kbar, so that muscovite may be a more important deep crustal H_2O reservoir than biotite.

KEY WORDS: *leucogranites; trondhjemites; Himalaya; anatexis; muscovite*

INTRODUCTION

Most peraluminous leucogranites are probably 'pure' crustal melts that are uncontaminated by mantle material. This conclusion is supported by: (1) radiogenic and stable isotopic compositions of peraluminous leucogranites; (2) their common field setting within medium- to high-grade regional metamorphic terranes; (3) lack of spatial and temporal associations between them and basaltic magmatism; and (4) experimental studies that have shown that melting of metasedimentary rocks generates peraluminous, silica-rich melts. Some of the best-known examples of peraluminous leucogranites are the Miocene intrusive bodies from the Himalayan orogen (e.g. Le Fort, 1981; Searle & Fryer, 1986; Le Fort *et al.*, 1987; Castelli & Lombardo, 1988; Stern *et al.*, 1989; Scaillet *et al.*, 1990; Inger & Harris, 1993). Despite many detailed studies of the Himalayan leucogranites, the heat source for crustal melting during regional metamorphism in the Himalayan orogen (e.g. Harris & Massey, 1994) and the role of fluids in magma generation [compare, e.g. France-Lanord & Le Fort (1988) with Harris *et al.* (1993)] are as yet unresolved questions. These uncertainties remain, in part, because of a lack of experimental results that constrain solidus temperatures, melting reactions, and melt and restite compositions of likely metamorphic protoliths for Himalayan leucogranites.

In this paper we describe the melting relations of two metapelitic rocks from the High Himalayan Crystalline Sequence (Inger & Harris, 1992), a muscovite schist (MS) and a tourmaline-bearing muscovite–biotite schist (MBS). These rocks are likely sources for Himalayan leucogranites (Harris *et al.*, 1993, 1995; Inger & Harris, 1993). Experiments were conducted at 6, 8 and 10 kbar and 700–900°C, both without added H_2O (dehydration-melting) and with 1–4 wt % added H_2O (H_2O-fluxed melting). Our results constrain the beginning of dehydration-melting in these pelitic schists, show how melt compositions and residual assemblages respond to

*Corresponding author. Telephone: 706-542-2394. Fax: 706-542-2425.
e-mail: klingon@3rdrock.gly.uga.edu

progressive breakdown of muscovite, and address the effects of H_2O infiltration during melting.

PREVIOUS EXPERIMENTAL STUDIES ON THE ORIGIN OF LEUCOGRANITE MAGMAS

The phase relations of leucogranite magmas have been addressed by melting and crystallization experiments on natural leucogranitic bulk compositions (Huang & Wyllie, 1973, 1981; Bénard *et al.*, 1985; Weidner & Martin, 1987; London *et al.*, 1989; Scaillet *et al.*, 1995). These workers have focused primarily on understanding the crystallization histories of leucogranites and pegmatites. Data from these studies constrain temperatures, melt fractions, and fugacities of H_2O and other volatile species during intrusion and crystallization of leucogranite magmas, but do not by themselves settle fundamental questions about their origin, such as pressure and temperature of melting and the role of externally derived fluids. This is so because the sources of leucogranite magmas, in the Himalaya and elsewhere, are more likely to have been metasedimentary rocks than other granitoid rocks. This conclusion is supported by the isotopic and trace element compositions of the leucogranites (e.g. Le Fort *et al.*, 1987; France-Lanord & Le Fort, 1988; France-Lanord *et al.*, 1988; Nabelek *et al.*, 1992; Inger & Harris, 1993; Harris *et al.*, 1995; Williamson *et al.*, 1996), as well as by the fact that metamorphic rocks of sedimentary derivation that pre-date leucogranite magmatism are abundant in orogenic belts, whereas granitoid rocks older than the leucogranites are relatively scarce or altogether absent (e.g. Le Fort, 1981, 1988; Inger & Harris, 1992; Nabelek *et al.*, 1992). The distinction between crystallization of leucogranites and melting of metasediments is important. Whereas K and Na in granitoid rocks reside predominantly in feldspars, in metasedimentary rocks they reside predominantly in micas and plagioclase, respectively. The latter assemblage responds to changes in pressure and H_2O activity differently from a two-feldspar assemblage (e.g. Patiño Douce, 1996). Melting experiments conducted with assemblages that are dominated by two feldspars + quartz are thus not accurate models for processes that take place in the source regions of leucogranite magmas (see Patiño Douce & Johnston, 1991; Patiño Douce, 1996). To arrive at an adequate understanding of leucogranite magmas, from their source region to their final emplacement site, it is necessary to combine results from melting experiments of metasedimentary rocks with those from crystallization experiments of leucogranites.

Most experimental melting studies of metasedimentary rocks have focused on compositions in which biotite was the only hydrous mineral (Le Breton & Thompson, 1988; Holtz & Johannes, 1991; Skjerlie & Johnston, 1993; Vielzeuf & Montel, 1994; Carrington & Harley, 1995; Patiño Douce & Beard, 1995, 1996; Dooley & Patiño Douce, 1996; Patiño Douce, 1996). A few experimental studies have used metasedimentary rocks that contained biotite and muscovite (Vielzeuf & Holloway, 1988; Patiño Douce & Johnston, 1991; Gardien *et al.*, 1995). Other experimental studies have used simplified assemblages and synthetic end-member compositions to model melting of metasedimentary rocks. These model systems include phlogopite + quartz (e.g. Peterson & Newton, 1989; Vielzeuf & Clemens, 1992), muscovite + quartz (Storre, 1972; Storre & Karotke, 1972) and muscovite + albite + quartz (Petö, 1976).

There have been no experimental melting studies of rocks in which muscovite is the dominant hydrous phase. Instead, the melting behavior of such rocks has been modeled by extrapolating from the experimental results of simple end-member systems (e.g. Thompson & Algor, 1977; Thompson, 1982; Clemens & Vielzeuf, 1987; Le Breton & Thompson, 1988). Although these extrapolations are a good first approximation to understanding the generation of peraluminous leucogranites, there is a clear need for direct experimental determination of solidus temperatures, phase relations and melt compositions produced from muscovite schists, during both dehydration-melting and H_2O-fluxed melting.

STARTING MATERIALS

Experiments were performed with two kyanite-zone metapelitic rocks from the hanging wall of the Main Central Thrust of the Himalayas (the High Himalayan Crystalline Sequence, Inger & Harris, 1992; Harris & Massey, 1994). Such rocks are the most likely source of Himalayan leucogranites because: (1) their modal compositions include sufficient mica and plagioclase to generate abundant granitic melt (Patiño Douce & Johnston, 1991), and (2) their Sr, Nd and O isotopic characteristics uniquely match those of Himalayan leucogranites (Harris & Massey, 1994; see also France-Lanord *et al.*, 1988). Bulk-chemical, modal and mineral compositions of the starting materials are given in Table 1. The felsic assemblage quartz + plagioclase + muscovite constitutes 93% of the muscovite schist (MS, sample N-13), which also contains ~5% garnet and ~2% biotite. The other rocks is a muscovite–biotite schist (MBS, sample PAN-3). Its assemblage consists of 78% quartz + plagioclase + muscovite, 13% biotite, 6% garnet, and about 1% each of tourmaline, staurolite and kyanite. Both samples were collected from near the base of the High Himalayan Crystalline Sequence in the hanging wall of the Main Central Thrust. Sample N-13 is from the Langtang valley

Table 1: Composition of starting material

	Modal contents	SiO_2	Al_2O_3	TiO_2	FeO*[1]	MgO	MnO	CaO	Na_2O	K_2O	F	Total
Muscovite schist (MS)												
Quartz	43	—	—	—	—	—	—	—	—	—	—	—
Plagioclase	28	64·13	22·08	—	0·04	—	—	3·02	9·99	0·11		99·36
Muscovite	22	48·13	34·45	1·18	1·07	1·24	0·06	0·01	0·71	9·63	0·20	96·60[2]
Biotite	2	35·34	17·78	3·23	20·40	9·86	0·04	0·00	0·16	9·13	0·68	96·31[2]
Garnet	5	36·48	21·25	0·01	33·20	3·67	2·60	1·81	—	—	—	99·02
Bulk rock		75·28	14·29	0·36	2·40	0·66	0·13	0·94	2·77	2·4	—	99·23
Muscovite–biotite schist (MBS)												
Quartz	38	—	—	—	—	—	—	—	—	—	—	—
Plagioclase	11	63·38	22·81	—	—	—	—	3·73	9·57	0·06	—	99·55
Muscovite	29	47·53	33·62	0·72	1·31	1·12	0·02	0·01	1·04	9·51	0·08	94·96[2]
Biotite	13	35·32	18·63	2·03	19·86	10·25	0·08	0·09	0·16	9·22	0·30	95·94[2]
Garnet	6	38·03	21·25	—	31·26	3·38	2·29	3·64	—	—	—	99·85
Ky + St + Tur[3]	4	—	—	—	—	—	—	—	—	—	—	
Bulk rock		67·03	16·26	0·79	5·50	1·88	0·14	1·06	1·36	3·39	—	97·41

Bulk compositions (wt %) determined with X-ray fluorescence (XRF) spectrometry of fused disks at the Open University. Phase compositions (wt %) determined with the electron microprobe at the University of Georgia (MS) and the Open University (MBS). Modal abundances determined by point counting of petrographic sections. —, not analyzed.
[1]Total Fe as FeO.
[2]F equivalents already subtracted.
[3]Total approximate modal abundance of kyanite + staurolite + tourmaline.

of the central Nepalese Himalaya, and sample PAN-3 is from the Zanskar region of the western Himalaya. Initial $^{87}Sr/^{86}Sr$ ratios for these samples (calculated at 20 Ma) are 0·7654 and 0·7609, respectively, which agree with typical values obtained for leucogranites from the Himalayan orogen (Harris & Ayres, 1997).

We infer that the bulk of the mineral assemblages in our starting materials approached equilibrium at $P \approx$ 8–10 kbar and $T \approx$ 700–750°C. Estimates of metamorphic P–T conditions were based on: (1) Fe–Mg exchange between garnet and biotite and (2) the reaction annite + anorthite = muscovite + grossular + almandine. We used the standard state thermodynamic properties of Berman (1988, 1990) and the solution models of Berman (1990) for garnet, Patiño Douce *et al.* (1993) for biotite and muscovite, and Fuhrman & Lindsley (1988) for plagioclase. Garnet and muscovite in sample MS are zoned (core compositions are given in Table 1), which yields two T–P intersections. These are T = 740°C and P = 10·5 kbar for core compositions, and T = 650°C and P = 8·5 kbar for rim compositions. No mineral zonations were detected in sample MBS, which yields a single T–P intersection of 730°C and 11 kbar. This result is, within error, identical to that obtained for MS core compositions. The P–T conditions inferred from core compositions in both rocks overlap those estimated by Inger & Harris (1992) for peak metamorphism of kyanite schist near the base of the High Himalayan Crystalline Sequence. The rim P–T estimates for MS are more difficult to interpret. This rock may have undergone relatively rapid cooling during decompression, which may explain why it lacks evidence for partial melting (see below).

One experiment was conducted with MBS plus 10 wt % added tourmaline, to constrain potential effects of this phase on dehydration-melting. For this experiment, a >95% pure tourmaline concentrate was separated by hand from a finely crushed fraction of MBS, and then added to the starting material.

EXPERIMENTAL AND ANALYTICAL PROCEDURES

Experimental apparatus and sample containment

Experiments were performed in solid-media piston-cylinder apparatus at the University of Georgia, with 0·5 inch diameter NaCl–graphite cell assemblies, at

Table 2: Experimental conditions, phase assemblages and abundances

Run no.	*P* (kbar)	*T* (°C)	Time (h)	H_2O[1] (wt %)	Qtz	Pl	Ms	Bt	Grt	Sil	Spl	St	Kfs	Melt
Muscovite schist (MS)														
APD-635	6	700	367	4	x	x	x	x	x	—	—	—	—	—
APD-605	6	750	360	0	x	x	x	x	x	x	—	—	—	tr
APD-639	6	750	276	1	37	23	22	2	5	0	0	0	0	11
APD-629	6	750	239	2	36	13	13	2	5	0	0	0	0	31
APD-601	6	775	342	0	42	25	15	3	5	1	0	0	1	8
APD-623	6	775	242	2	31	15	4	3	4	2	1	0	0	40
APD-596	6	800	385	0	38	26	6	5	4	3	0	0	2	16
APD-611	6	820	318	0	35	21	0	4	4	5	0	0	5	25
APD-599	6	850	285	0	33	22	0	3	5	4	0	0	4	28
APD-626	6	900	200	0	32	22	0	1	9	4	0	0	0	32
APD-643	8	800	333	0	43	26	15	3	5	1	0	0	1	6
APD-634	10	700	391	4	37	24	25	0	7	0	0	0	0	8
APD-637	10	750	262	1	38	23	21	2	5	0	0	0	0	12
APD-630	10	750	265	2	32	12	16	2	6	1	0	0	0	31
APD-641	10	775	243	4	30	7	16	0	4	0	0	1	0	43
APD-622	10	820	338	0	x	x	x	x	x	—	—	—	—	—
APD-638	10	835	320	0	41	24	18	4	5	2	0	0	tr	6
APD-620	10	850	248	0	36	22	2	3	5	4	0	0	4	23
APD-624	10	900	275	0	34	20	0	1	9	4	0	0	5	27
Muscovite–biotite schist (MBS)[2]														
APD-650	6	725	339	0	x	x	x	x	x	x	—	x	—	—
APD-648	6	750	318	0	36	8	22	16	6	2	—	1	1	8
APD-649	10	795	312	0	x	x	x	x	x	x	—	x	tr	tr
APD-646	10	820	289	0	29	4	10	19	7	4	—	2	6	19
APD-652[3]	10	820	288	0	x	—	x	x	x	x	—	x	x	20
APD-661[4]	10	820	289	0	28	3	0	24	7	5	—	2	7	24

x, phase is present but its abundance was not determined; —, phase is absent; tr, trace amounts, but abundance was not determined. In all other cases, phase abundances (wt %) were determined by a combination of mass-balance and analysis of BSE images (see text). Mineral abbreviations after Kretz (1983).
[1]Added H_2O.
[2]Runs APD-650, APD-649, and APD-652 also contain tourmaline.
[3]Experiment with 10% added tourmaline. Phase abundances cannot be calculated by mass-balance; melt abundance was estimated by point-counting BSE image.
[4]Crystallization experiment. Temperature was initially held at 980°C for 98 h, then lowered to 820°C. Run duration shown corresponds to the time at this final temperature.

700–900°C and 6, 8 and 10 kbar, with run durations of 8–16 days (Table 2). The apparatus, experimental techniques, and *P*–*T* uncertainties (±0·5 kbar, ±5°C) have been described in detail by Patiño Douce & Beard (1994, 1995, 1996) and Patiño Douce (1995). Starting materials were ground for 1 h in a shatter box with WC lining and balls. The grain size of most of the material was ≤10 μm, but some larger grains of muscovite (up to 30 μm long) remained. Samples were placed in welded Au capsules of 2·4 mm inner diameter, with a 0·3 mm thick wall. The capsules contained either 6 mg of dry sample (dehydration-melting experiments) or 10 mg of dry sample plus H_2O, added with a microsyringe (experiments with 1–4 wt % added H_2O). The capsules used in dehydration-melting experiments were loaded and then stored open in an oven at 130°C for at least 24 h, to eliminate adsorbed humidity. They were then crimped inside the oven and immediately sealed by arc welding. Weight loss of capsules with added H_2O was monitored during welding, and the capsules were also checked for leaks before the experiments by verifying that no weight loss (±0·1 mg) occurred after ~2 h in an

oven at 130°C. Capsules were examined for tears and weighed after the experiments. Weight losses of $\geq 0{\cdot}1$ mg were not detected in any of the experiments.

To study whether micas persist metastably in melting experiments and, if so, how this affects melt compositions, we also performed a crystallization experiment with starting material MBS. This charge was initially heated to 980°C at 10 kbar, and the temperature was held at this value for 4 days. The temperature was then lowered to a final value of 820°C at a rate of 50°C/min, while manually maintaining the pressure constant at 10 kbar. The final T and P conditions (820°C, 10 kbar) were then held constant for an additional period of 12 days.

No attempt was made to buffer $f(O_2)$ in the experiments, because the graphite-based cell assemblies that we used restrict $\log f(O_2)$ in the samples to between QFM (quartz–fayalite–magnetite) and QFM − 2. The stabilities and compositions of ferromagnesian phases coexisting with silicic melts are not significantly affected by $f(O_2)$ variations within this range (Patiño Douce & Beard, 1994, 1995, 1996; Patiño Douce, 1996).

Analytical procedures

Phase compositions were determined using the JEOL JXA 8600 electron probe microanalyzer at the University of Georgia, with an accelerating voltage of 15 kV and sample current of 5 nA. To minimize alkali migration, and also to insure accurate targeting, glass analyses were performed in scanning mode at 50 000 × magnification, with a focused beam rastered over an area of approximately 4 μm × 4 μm. All other phases were also analyzed in scanning mode but with magnifications typically >100 000 ×, resulting in analyzed areas ≤2 μm × 2 μm. Na and K were counted first, and Na was counted for 10 s. All other elements were counted for 40 s. Variations of K and Na count-rates with time were investigated for several of the experimental run products that contained >20% melt (Table 2), by analyzing neighboring areas of glass for time intervals ranging from 1 to 40 s. No count-rate decay was detected for K. The count-rate decay of Na depends on the H_2O content of the glass, which was inferred from the difference between analyzed wt % total and 100. By extrapolating the Na count-rate decay to time 0, we calculated correction factors ranging from ~20 to ~50% for Na concentrations in glasses in which the totals ranged from 97 to 91 wt %, respectively. In experimental run products that contained <20% melt it was not generally possible to find large enough areas of glass to determine the decay of count rates. Correction factors for these glasses were those determined for high melt fraction experimental run products with similar analytical totals. In experiments with sample MBS, we attempted to analyze B in the glasses, using a synthetic layered crystal with 2d spacing of 148 Å, and either synthetic boron nitride or synthetic borosilicate glass (National Institute of Science and Technology, number 93A) standards. We obtained detection limits of the order of 1·5 wt % B_2O_3. Glass analyses from MBS runs at 10 kbar, 820°C (Table 3) yielded B_2O_3 concentrations in the range 1·5–2·5 wt %, i.e. barely above detection limit. We estimate B_2O_3 in these glasses to be 2 wt %. Glass in the MBS experiment performed at 6 kbar, 750°C yielded B values below our detection limit.

Phase abundances in the experimental run products (Table 2) were calculated by a combination of mass balance and partial estimates of modal abundances obtained from back-scattered electron (BSE) images [the method has been described more fully by Patiño Douce & Johnston (1991)]. We carried out mass balance using values for K_2O, TiO_2, Al_2O_3, SiO_2, MgO, CaO, and FeO*. Estimates of modal abundances of melt and total mafic phases, obtained by point-counting BSE images, were included as additional linear equations in the least-squares minimization routine, and were given the same weight as the chemical mass-balance equations. This method yielded a total of nine linear equations, which were solved by either least-squares fitting of 5–8 phases (MS experiments) or exact solution for nine phases (MBS experiments). Analytical errors and the presence of zoned phases generated uncertainties in the calculated modes of ± ~2 wt % [see also Patiño Douce (1995)].

DESCRIPTION OF EXPERIMENTAL PRODUCTS AND MINERAL COMPOSITIONS

Glass

Glass (quenched melt) occurs in regions that range in size from <2 μm in near-solidus experiments to 10–20 μm in experiments with the highest melt fractions (Table 2, Fig. 1). In the dehydration-melting experiments, glass is intergrown with euhedral crystals of K-feldspar, aluminosilicate, and biotite (Fig. 1a, c and d). This texture results from simultaneous growth of all of the products of incongruent melting of muscovite, and is absent from experiments with added H_2O (compare Fig. 1b). Melt compositions within each run product are remarkably uniform, regardless of its melt fraction (Table 3).

Quartz and aluminosilicate minerals

Quartz is abundant in all experimental run products. It occurs as globular crystals up to 10 μm across. An aluminosilicate phase is present in the products of all

Table 3: Glass compositions (wt %)

P (kbar)	*T*(°C)	H_2O (wt %)	SiO_2	Al_2O_3	TiO_2	FeO*[1]	MgO	MnO	CaO	Na_2O[2]	K_2O	Total[3]	A/CNK[4]	Na/K[5]	*n*
Muscovite schist (MS)															
6	750	1	74·95	15·73	0·14	1·01	0·34	0·04	0·56	4·53	2·70	93·77	1·38	1·68	6
6	750	2	74·70	15·99	0·10	0·87	0·35	0·04	0·77	4·18	3·01	93·50	1·39	1·39	6
6	775	0	75·43	15·04	0·17	0·76	0·18	0·04	0·52	3·57	4·29	96·20	1·31	0·83	4
6	775	2	74·65	15·55	0·11	0·76	0·26	0·06	0·61	3·79	4·20	95·54	1·31	0·90	7
6	800	0	74·09	15·86	0·15	1·00	0·21	0·05	0·49	3·22	4·91	96·79	1·38	0·66	4
6	820	0	74·94	14·95	0·11	0·90	0·24	0·04	0·47	3·72	4·62	97·15	1·25	0·80	8
6	850	0	74·30	15·01	0·15	0·94	0·24	0·06	0·46	3·85	4·99	97·86	1·19	0·77	10
6	900	0	73·80	15·13	0·29	0·86	0·39	0·03	0·42	3·88	5·19	98·54	1·19	0·75	10
8	800	0	74·14	15·95	0·12	0·99	0·34	0·03	0·62	3·86	3·95	94·28	1·36	0·98	5
10	700	4	73·20	16·01	0·04	0·70	0·19	0·02	1·46	6·67	1·71	93·93	1·03	3·90	6
10	750	1	74·47	16·00	0·08	0·71	0·19	0·02	0·87	5·74	1·91	91·45	1·22	3·01	7
10	750	2	73·66	16·36	0·06	0·66	0·41	0·02	1·41	5·32	2·11	93·86	1·20	2·52	9
10	775	4	73·75	15·75	0·03	0·74	0·41	0·03	1·52	5·82	1·94	90·20	1·09	3·00	10
10	835	0	73·68	16·17	0·19	0·75	0·25	0·05	0·61	4·92	3·40	94·66	1·25	1·45	6
10	850	0	73·80	16·07	0·15	0·73	0·20	0·02	0·65	3·61	4·77	95·84	1·31	0·76	8
10	900	0	73·40	15·25	0·24	0·74	0·35	0·07	0·52	4·35	5·08	97·47	1·12	0·86	10
Muscovite–biotite schist (MBS)[6]															
6	750	0	75·60	15·23	0·06	1·05	0·17	0·02	0·82	3·17	3·88	94·67	1·40	0·82	4
10	820	0	74·43	15·76	0·19	1·08	0·39	0·05	1·05	3·21	3·82	92·14	1·39	0·84	9
10	820[7]	0	74·49	15·90	0·13	0·98	0·26	0·04	1·01	3·17	3·91	93·67	1·41	0·81	8
10	820[8]	0	74·52	15·65	0·13	1·03	0·32	0·02	1·15	3·07	4·11	93·05	1·35	0·75	10

Recalculated to 100 wt % anhydrous. Values reported are averages of the number of analyses shown, of different areas of glass. Relative analytical uncertainties (±2 SD of the average values) are better than: SiO_2, 1%; Al_2O_3, 2%; TiO_2, 10%; FeO*, 8%; MgO, 10%; MnO, 100%; CaO, 12%; Na_2O, 18%; K_2O, 5%. *n*, number of analyses.
[1]Total Fe as FeO.
[2]Includes correction for Na volatilization—see text.
[3]Original probe total.
[4]$Al_2O_3/(CaO + Na_2O + K_2O)$, molar.
[5]Na_2O/K_2O, wt %.
[6]Glasses in the MBS melting and crystallization experiments at 10 kbar, 820°C contain ~2 wt % B_2O_3 (semi-quantitative determination, see text). Probe totals listed do not include this estimated B_2O_3 content.
[7]Experiment with 10% added tourmaline.
[8]Crystallization experiment.

dehydration-melting experiments, regardless of the starting material. It occurs as acicular crystals that vary from $\ll 1$ μm to 4 μm in width, and that are intergrown with euhedral K-feldspar crystals and minute euhedral crystals of biotite (Fig. 1a). Microprobe analyses of large grains confirm that they are stoichiometric Al_2SiO_5. The stable polymorph at the P–T conditions of all dehydration-melting experiments is sillimanite, and euhedral basal sections of sillimanite are present in most of these run products (e.g. Fig. 1a). Scarce crystals of an aluminosilicate phase are also present in a few MS experiments with added H_2O (Table 2).

Muscovite

Muscovite occurs in MS experimental run products at $T \leq 800$°C (at 6 kbar), $T = 800$°C (at 8 kbar), and $T \leq 850$°C (at 10 kbar). It forms large (~10 μm), generally anhedral, relict grains. Muscovite crystals are also present in melting experiments with MBS, except in the one to which 10% tourmaline was added. Muscovite did not form in the crystallization experiment on MBS at $T = 820$°C, $P = 10$ kbar, even though it is present in the melting experiment at the same conditions. Muscovite compositions in all the experimental run products are indistinguishable from those of the starting materials [see

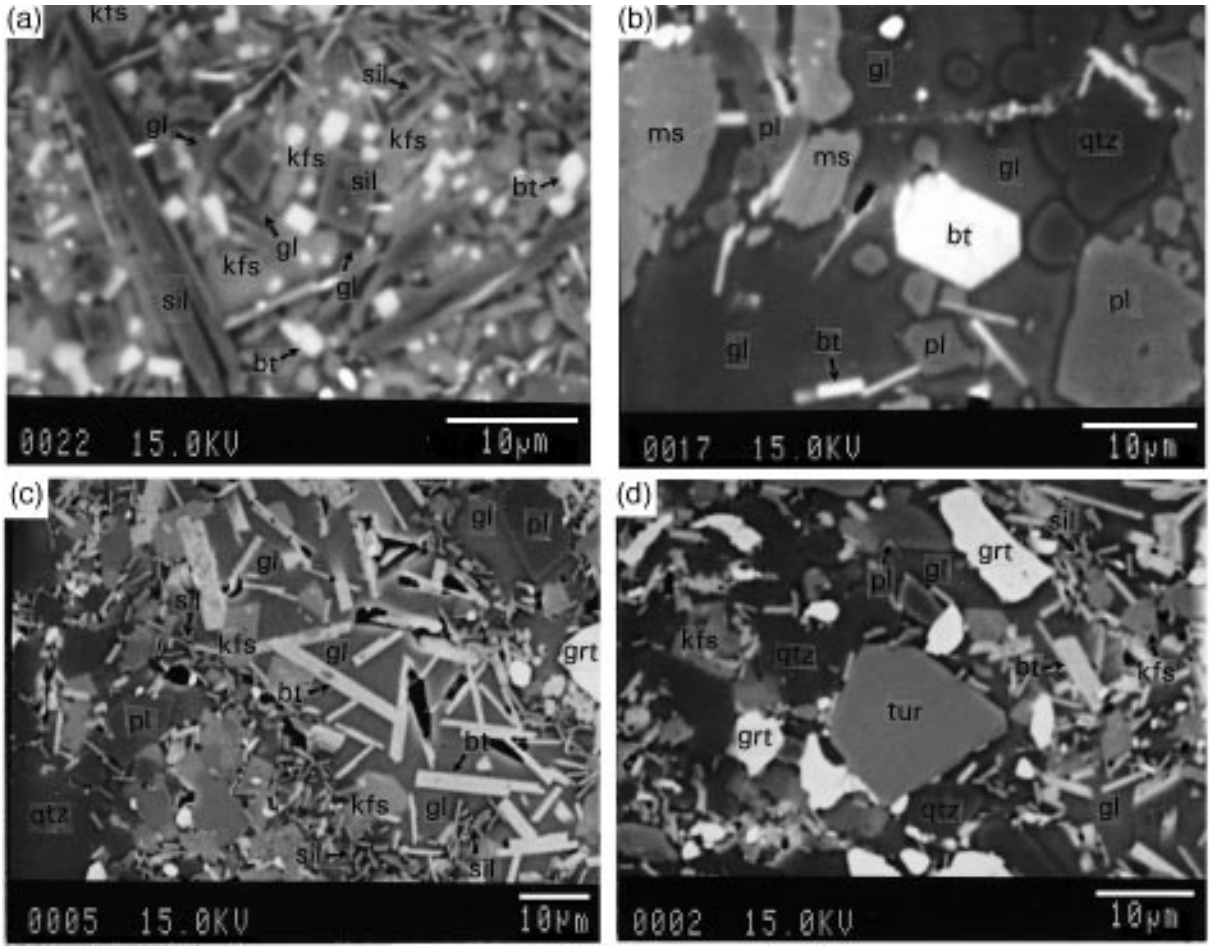

Fig. 1. Back-scattered electron (BSE) images of selected run products. Mineral abbreviations after Kretz (1983), except gl: glass. (a) APD-596, dehydration-melting of MS at 6 kbar, 800°C. Typical aggregate of sillimanite + K-feldspar + biotite + glass, formed by incongruent breakdown of a large (>10 μm across) muscovite grain. (b) APD-629, melting of MS with 2 wt % added H_2O, at 6 kbar, 750°C. [Note large area of glass, relict muscovite and absence of typical texture formed by dehydration-melting; compare panel (a).] (c) APD-646, dehydration-melting of MBS at 10 kbar, 820°C. Another example of the texture and mineral assemblage formed by incongruent breakdown of muscovite. (d) APD-652, dehydration-melting of MBS + 10% added tourmaline at 10 kbar, 820°C. (Note idiomorphic tourmaline crystal and xenomorphic garnet crystals, the latter indicating that garnet is an inert phase before the onset of the biotite dehydration-melting reaction.)

also Scaillet *et al.* (1995)], hence no compositions are reported. Given that muscovite is absent from the crystallization experiment and that its composition does not change in melting experiments, it appears likely that this phase may persist metastably in melting experiments [see also Huang & Wyllie (1981) and Scaillet *et al.* (1995)].

Biotite

Biotite is present in all experimental run products, except in those with MS plus 4 wt % added H_2O at $P = 10$ kbar, $T = 700$ and 775°C. In the products of dehydration-melting experiments, as well as in the crystallization experiment with MBS, it occurs predominantly as small subhedral flakes ≤ 5 μm wide (Fig. 1a, c and d). However, euhedral grains as large as 10 μm are found in some experimental run products with added H_2O (Fig. 1b). In the products of experiments at $T \leq 750$°C, biotite crystals are notably smaller than in those resulting from higher temperature experiments. The compositions of these smaller biotite grains (Table 4) may not always represent uncontaminated analyses. Biotite from run products is more aluminous and generally has higher Mg/Fe ratio than biotite in the starting materials (Table 4).

Garnet

Garnet is present in all run products of both starting materials. There is a striking difference, however, between garnet from experimental run products of MS at 900°C, 6 and 10 kbar, and garnet from all other (lower

Table 4: Representative compositions of ferromagnesian phases (wt %)

P (kbar)	*T* (°C)	H_2O (wt %)	SiO_2	Al_2O_3	TiO_2	FeO*[1]	MgO	MnO	CaO	Na_2O	K_2O	F	Total[2]	*mg*-no.	*n*
Biotite (muscovite schist, MS)															
6	750	0	36·93	21·10	3·24	15·46	9·41	0·13	0·02	0·46	8·87	0·74	96·03	52·0	5
6	750	1	41·48	20·53	2·91	12·89	8·58	0·05	0·12	0·70	7·57	0·43	95·08	54·3	5
6	750	2	38·47	21·06	2·93	13·23	11·08	0·03	0·06	0·55	8·57	0·40	96·19	59·9	5
6	775	0	37·33	21·47	3·85	15·18	8·61	0·21	0·03	0·44	9·12	0·79	96·67	50·3	5
6	775	2	37·66	21·24	3·05	13·69	10·03	0·10	0·03	0·44	8·90	0·71	95·55	56·6	5
6	800	0	38·71	21·45	3·19	15·47	9·09	0·24	0·05	0·63	9·05	1·09	98·49	51·2	5
6	820	0	36·44	18·78	3·39	15·76	11·41	0·12	0·01	0·41	9·13	1·13	96·10	56·3	5
6	850	0	37·33	19·39	3·21	13·20	13·05	0·09	0·01	0·55	9·21	1·32	96·80	63·8	5
6	900	0	38·56	18·46	5·53	8·32	15·69	0·11	0·02	0·71	9·09	1·20	97·18	77·1	5
8	800	0	36·76	20·72	3·19	13·92	10·00	0·01	0·02	0·40	8·98	0·37	94·19	56·2	5
10	750	1	36·01	19·56	3·29	16·38	10·45	0·08	0·01	0·33	9·24	0·54	95·64	53·2	5
10	750	2	37·37	19·11	3·48	16·16	10·66	0·00	0·03	0·27	8·25	0·38	95·55	54·0	5
10	820	0	36·23	20·89	3·64	14·35	9·65	0·12	0·01	0·31	9·39	0·80	95·05	54·5	5
10	835	0	37·65	21·66	3·45	12·14	11·39	0·00	0·03	0·52	9·26	0·94	96·64	62·6	5
10	850	0	37·13	19·75	3·38	13·40	11·51	0·11	0·02	0·48	9·38	1·05	95·76	60·5	5
10	900	0	37·18	18·63	5·05	10·01	14·30	0·00	0·01	0·58	9·23	1·26	95·73	71·8	5
Biotite (muscovite–biotite schist, MBS)															
6	750	0	35·95	22·11	1·71	16·87	8·63	0·05	0·05	0·32	8·23	0·41	94·16	47·7	5
10	820	0	37·30	21·28	2·83	14·20	9·63	0·08	0·03	0·29	8·63	0·65	94·62	54·7	5
10	820[3]	0	37·97	20·92	3·30	14·91	9·36	0·00	0·01	0·24	8·90	0·67	96·00	52·6	5
10	820[4]	0	38·75	21·33	4·01	12·67	10·35	0·00	0·05	0·36	8·77	0·51	96·29	59·3	5
Garnet (muscovite schist, MS)															
6	900	0	41·83	23·31	0·32	22·11	12·09	0·70	1·02	—	—	—	101·37	49·4	3
10	900	0	39·39	22·64	0·34	24·44	10·71	0·44	1·31	—	—	—	99·24	43·8	3
Spinel (muscovite schist, MS)															
6	775	2	0·65	60·89	0·13	27·83	7·28	0·20	0·03	—	—	—	96·99	31·8	1
Staurolite (muscovite schist, MS)															
10	775	4	27·16	55·51	0·74	10·12	3·25	0·05	0·03	—	—	—	96·87	36·4	3
Staurolite (muscovite–biotite schist, MBS)															
6	750	0	27·11	53·51	0·73	12·24	1·98	0·00	0·00	—	—	—	95·57	22·4	3
10	820	0	27·93	53·87	0·76	11·80	3·11	0·04	0·00	—	—	—	97·51	32·0	3
10	820[3]	0	28·49	54·20	0·68	11·93	2·83	0·17	0·02	—	—	—	98·32	29·7	3
10	820[4]	0	28·16	53·55	0·72	11·04	3·07	0·03	0·00	—	—	—	96·64	33·1	3
Tourmaline (muscovite–biotite schist, MBS)															
10	820[3]	0	35·71	33·60	0·46	10·61	3·12	0·11	0·17	1·89	0·11	0·39	85·98	34·4	3

Values are averages of the number of analyses shown, of different grains. Relative analytical uncertainties (±2 SD of the average values) are better than: SiO_2, 2%; Al_2O_3, 2%; TiO_2, 10% (for biotite only); FeO*, 5%; MgO, 5%; MnO, 30%; CaO, 5% (for garnet only); Na_2O, 15%; K_2O, 5%; F, 15%. Uncertainties for spinel are unknown. *mg*-no. = MgO/(MgO+FeO), molar proportions. *n*, number of analyses.

[1]Total Fe as FeO.

[2]F equivalent already subtracted from reported totals.

[3]Experiment with 10% added tourmaline.

[4]Crystallization experiment.

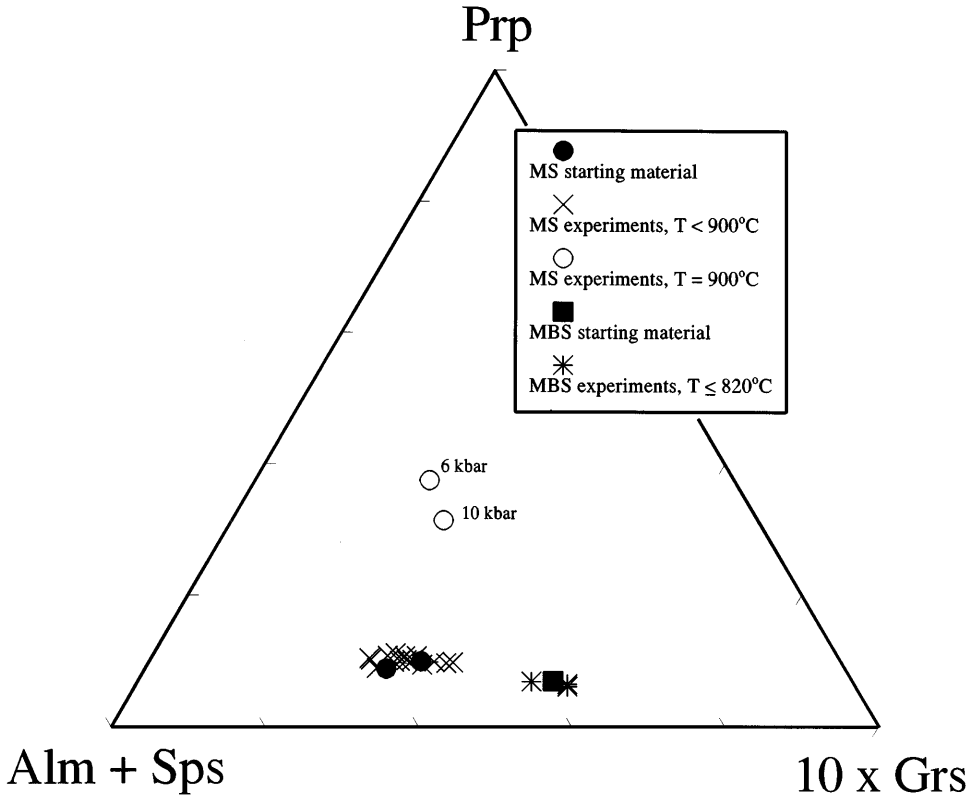

Fig. 2. Garnet compositions in experimental run products. Molar proportions of pyrope (Prp), grossular (Grs) and almandine + spessartine (Alm + Sps). It should be noted that only garnet in run products at 900°C departs in composition from those in the starting materials, denoting the onset of the biotite dehydration-melting reaction.

temperature) experiments. Garnet crystals in the products of the two highest temperature experiments display wide ($\geq$5 μm) euhedral rims, with higher pyrope and lower almandine and spessartine contents than garnet of the starting material (Table 4, Fig. 2). Grossular contents in these high-temperature garnet rims increase slightly from 6 to 10 kbar (Fig. 2). In all other experiments, garnet is anhedral or very poorly subhedral. Narrow neoblastic rims were observed in one MS experiment at P = 10 kbar, T = 700°C, with 4 wt % added H_2O. The compositions of garnet from experimental run products of both MS and MBS at T < 900°C overlap those present in the starting materials (hence the former are not reported in Table 4, but are shown in Fig. 2). Garnet abundances (Table 2) exceed those in the starting materials only in the two 900°C experiments with MS (about twice the starting abundance), and in the MS experiment at 700°C, 10 kbar, with 4 wt % added H_2O (about 1·5 times the starting abundance).

Plagioclase

Plagioclase is abundant in all experimental run products, but has different characteristics in MS and MBS experiments. In MS run products, plagioclase occurs predominantly as 10 μm crystals composed of anhedral relict cores overgrown by well-developed, euhedral to subhedral rims, that are always more potassic than the cores. Some of the MS experimental run products at T $\geq$ 850°C show such rims along with 2–5 μm, subhedral, homogeneous crystals of the same composition. The compositions of the rims and of the small homogeneous crystals vary regularly with T and P (Table 5). Their orthoclase and anorthite contents increase and their albite content decreases with increasing temperature. Anorthite content is generally higher in experiments with added H_2O than in dehydration-melting experiments at similar P–T conditions (Table 5). In MBS experiments large plagioclase grains with the same composition as that of the starting material are rimmed by K-feldspar rather than plagioclase.

Potassium feldspar

Potassium feldspar is present in all but one (900°C at 6 kbar with MS) of the dehydration-melting experiments. It is absent from all experiments to which H_2O was

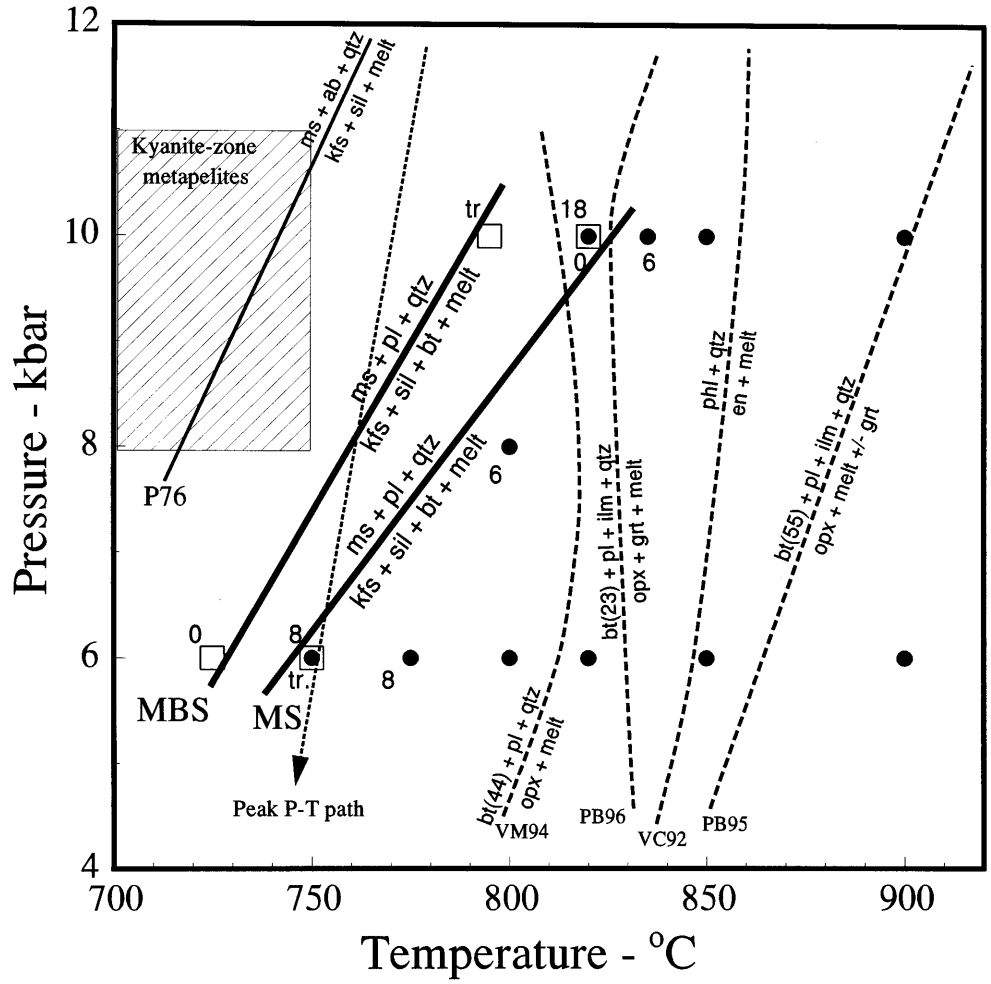

Fig. 3. Comparison of muscovite and biotite dehydration-melting solidi, and thermal conditions in the Himalayan orogen [mineral abbreviations after Kretz (1983)]. The experimentally determined dehydration-melting solidi for MS and MBS are shown with bold continuous lines. The filled circles and open squares are *P–T* conditions of dehydration-melting experiments on MS and MBS, respectively; the numbers are melt fractions in experimental run products that constrain the solidus (see Table 2). The fine continuous line labeled 'P76' is the dehydration-melting solidus for end-member muscovite + albite + quartz, determined by Petö (1976). The dashed lines are solidi for dehydration-melting of biotite (with *mg*-number in parentheses) + plagioclase + quartz in bulk compositions lacking muscovite and an aluminosilicate phase, as follows: VM94, Vielzeuf & Montel (1994), *mg*-number 44, no ilmenite; PB96: Patiño Douce & Beard (1996), *mg*-number 23, with ilmenite; VC92: Vielzeuf & Clemens (1992), end-member phlogopite + quartz; PB95: Patiño Douce & Beard (1995), *mg*-number 55, with ilmenite. The box with diagonal ruling shows the estimated *P–T* conditions for the Himalayan kyanite-zone metapelites. It should be noted that these *P–T* conditions do not intersect the experimentally determined solidi, which is consistent with the fact that the starting materials MS and MBS do not show indications of melting. The arrow is the adiabatic decompression path proposed by Harris & Massey (1994) for rocks that achieved the highest temperatures in the Himalayan orogen. [Note that this path intersects the solidi for MS and MBS at 6–8 kbar and ~750°C (see text).]

added. K-feldspar occurs as euhedral crystals ≤ 5 μm across (Fig. 1a and c). In some cases, these crystals appear to be isolated within areas of glass, but more commonly they are intergrown with sillimanite needles and minute biotite flakes, in fine-grained aggregates that partially or totally replace muscovite crystals (Fig. 1a and c). The anorthite contents of K-feldspar are low (<4 mol %), but both the anorthite and albite contents generally increase with temperature (Table 5). The abundance of K-feldspar increases with temperature, as does the melt fraction, if muscovite is present. Above the muscovite-out boundary, the abundance of K-feldspar decreases with increasing temperature (Table 2). These relationships, together with the textural features illustrated in Fig. 1a and c, show that K-feldspar is a product of the incongruent dehydration-melting reaction of muscovite.

Table 5: Representative compositions of feldspars (wt %)

P (kbar)	*T* (°C)	H_2O (wt %)	SiO_2	Al_2O_3	FeO*[1]	CaO	Na_2O	K_2O	Total	Ab[2]	An	Or	*n*
Neoblastic plagioclase (muscovite schist, MS)													
6	750	0	65·41	22·45	0·06	2·95	9·32	0·13	100·32	84·4	14·8	0·8	3
6	750	1	64·37	22·24	0·03	3·25	9·76	0·47	100·12	82·2	15·1	2·6	3
6	750	2	63·83	23·47	0·14	4·56	6·91	0·64	99·56	70·1	25·6	4·3	4
6	775	0	64·75	22·07	0·11	3·32	8·71	1·29	100·25	76·4	16·1	7·5	5
6	775	2	63·07	23·57	0·11	4·58	7·89	0·73	99·96	72·4	23·2	4·4	5
6	800	0	65·70	21·86	0·10	3·00	8·13	1·77	100·56	74·2	15·1	10·6	4
6	820	0	65·32	21·35	0·18	3·17	7·80	2·27	100·08	70·6	15·8	13·5	3
6	850	0	64·87	22·28	0·05	3·22	8·32	1·65	100·39	74·4	15·9	9·7	5
6	900	0	64·57	21·97	0·15	3·32	6·99	2·53	99·53	66·7	17·5	15·8	4
8	800	0	65·03	22·07	0·10	3·12	8·82	1·11	100·24	78·2	15·3	6·5	3
10	700	4	65·50	22·13	0·13	2·93	9·89	0·27	100·83	84·7	13·8	1·5	4
10	750	1	63·89	22·47	0·12	3·17	9·72	0·09	99·44	84·3	15·2	0·5	4
10	750	2	64·40	22·60	0·09	3·21	8·99	0·28	99·57	82·1	16·2	1·7	4
10	775	4	63·79	22·95	0·15	3·84	9·16	0·21	100·08	80·2	18·6	1·2	4
10	820	0	65·27	22·14	0·19	2·95	9·31	0·53	100·38	82·5	14·4	3·1	5
10	835	0	63·79	22·64	0·20	3·19	8·97	1·31	100·09	77·4	15·2	7·4	3
10	850	0	64·88	21·97	0·12	3·06	8·29	1·89	100·21	73·8	15·1	11·1	3
10	900	0	64·33	22·08	0·07	3·26	7·51	2·56	99·81	68·3	16·4	15·3	4
Alkali feldspar (muscovite schist, MS)													
6	775	0	64·67	21·32	0·09	0·67	3·41	10·20	100·37	32·5	3·6	63·9	5
6	800	0	67·54	17·94	0·16	0·26	2·78	10·06	98·74	29·1	1·5	69·4	5
6	820	0	66·31	18·95	0·12	0·37	3·47	11·27	100·49	31·3	1·8	66·9	5
6	850	0	65·54	20·65	0·15	0·40	3·63	9·77	100·14	35·3	2·2	62·5	5
10	835	0	67·38	18·60	0·09	0·34	2·73	10·07	99·21	28·6	1·9	69·4	5
10	850	0	66·06	19·78	0·12	0·40	3·39	10·88	100·62	31·5	2·1	66·5	5
10	900	0	67·07	19·38	0·21	0·65	3·96	9·42	100·67	37·6	3·4	59·0	5
Alkali feldspar (muscovite–biotite schist, MBS)													
10	820	0	64·36	19·84	0·37	0·33	2·23	12·64	99·77	20·8	1·7	77·5	4
10	820[3]	0	64·53	19·99	0·41	0·19	1·95	12·66	99·73	18·8	1·0	80·2	5
10	820[4]	0	66·54	19·02	0·45	0·30	2·13	12·56	101·07	20·2	1·6	78·3	4

Values are averages of the number of analyses shown, of different euhedral grains and/or idiomorphic rims (for plagioclase only, see text). Relative analytical uncertainties ($\pm$2 SD of the average values) are better than: SiO_2, 2%; Al_2O_3, 2%; FeO*, 20%; CaO, 5%; Na_2O, 5%; K_2O, 5%. *n*, number of analyses.
[1]Total Fe as FeO.
[2]Albite, anorthite and orthoclase contents, in molar proportions.
[3]Experiment with 10% added tourmaline.
[4]Crystallization experiment.

Spinel

Spinel is only present in one experimental run product of MS (6 kbar, 775°C with 2 wt % added H_2O). It occurs as scarce euhedral crystals $\leq$3 μm in diameter that are intergrown with sillimanite and biotite. Brearley & Rubie (1990) suggested that spinel is a metastable product of muscovite breakdown.

Staurolite

Staurolite is present in one experimental run product of MS (10 kbar, 775°C with 4 wt % added H_2O), in the products of all dehydration-melting experiments on MBS, and also in the crystallization experiment on MBS (Tables 2 and 4). It occurs as prismatic euhedral crystals 5–10 μm long that do not appear to be relict grains. Staurolite

in MBS experiments is significantly more magnesian at 10 kbar, 820°C than at 6 kbar, 750°C, and staurolite compositions in the melting and crystallization experiments at 10 kbar, 820°C are virtually identical (Table 4). These textural and compositional characteristics suggest that staurolite might be a stable phase at the P–T conditions of the experiments, even though staurolite is commonly thought to disappear from metamorphic rocks at a lower temperature than that at which muscovite breaks down.

Tourmaline

Tourmaline is found in sub-solidus and near-solidus experiments with MBS (6 kbar, 725°C; 10 kbar, 795°C), as well as in the experiment with MBS plus 10 wt % added tourmaline at 10 kbar, 820°C. In the former two experiments it is very scarce (<1 wt %), fine grained, and anhedral. In the latter, it is abundant (5–10%) and displays euhedral crystal faces (Fig. 1d) that show that this mineral recrystallized during the experiment. The stability of tourmaline at temperatures as high as 820°C is consistent with the experimental findings of Bénard *et al.* (1985) and of Scaillet *et al.* (1995). These workers showed that tourmaline can be a liquidus phase in both H_2O-saturated and H_2O-undersaturated leucogranite magmas.

APPROACH TO EQUILIBRIUM

Zoned crystals of plagioclase and garnet are present in our experimental run products, showing that equilibrium was not attained throughout the entire volume of the capsules. In addition, muscovite is present in the melting experiment with MBS at $P = 10$ kbar, $T = 820$°C, but not in the crystallization experiment with the same starting material and at the same P–T conditions. These observations underscore the fact that equilibrium in H_2O-poor experimental runs at $T < 800$°C is not attained readily (e.g. Brearley & Rubie, 1990). However, determining the melting behavior of natural metasedimentary rocks under H_2O-deficient conditions is essential if we are to understand the origin of leucogranite magmas. Because the melting behavior of such complex systems can be addressed only through experiments, we must examine the extent to which the results of imperfectly equilibrated experiments approach those of melting in nature.

The dehydration-melting solidus temperatures determined in the experiments (Fig. 3) are probably good approximations to the temperatures at which dehydration-melting would begin in nature in the rocks that we studied. This is suggested by the strong effects of pressure and composition on the temperatures at which melt is first observed in both starting materials (Fig. 3, Table 2). For example, the beginning of dehydration-melting in MS at 10 kbar takes place at higher temperature than that at which muscovite disappears from this bulk composition at 6 kbar (Table 2). If muscovite breakdown in the experiments were controlled solely by kinetics, rather than by phase equilibrium, this strong effect of pressure, which was also pointed out by Huang & Wyllie (1981), would not be observed. In addition, the beginning of dehydration-melting in MBS takes place at temperatures 15–30°C lower than in MS (Fig. 3). This displacement of the solidus is consistent with compositional effects on muscovite stability (see below).

Glass compositions determined in the melting experiments are also likely to approach equilibrium melt compositions. Glass compositions are homogeneous throughout the volume of the experimental charges, even in near-solidus experiments with low melt fractions. The compositions of plagioclase rims adjacent to glass areas, and of alkali feldspar and biotite crystals intergrown with glass, vary regularly with changes in temperature and pressure. These features suggest that equilibrium was at least locally attained in the melting experiments. Moreover, a comparison of glass compositions in the melting and crystallization experiments on MBS at $P = 10$ kbar, $T = 820$°C shows that, even if some muscovite persists metastably in the melting experiments, the effect on melt compositions is minor (Table 3). The fact that melt compositions in the melting and crystallization experiments are almost identical, even though muscovite is absent from the latter, indicates that muscovite coexisting with plagioclase and quartz breaks down incongruently to the same assemblage (K-feldspar + aluminosilicate + biotite + melt) and in very nearly the same proportions, regardless of whether or not equilibrium is attained.

We conclude that melting experiments provide reliable information on the solidus temperatures of muscovite schists, on the compositions of the melts that they produce, and on the nature and stoichiometry of the melting reactions. However, metastable persistence of muscovite in the melting experiments lowers the amount of melt that is produced (Table 2). The melt fractions observed in the melting experiments may thus not be representative of the melt fractions that would be produced in nature at the same P–T conditions.

DISCUSSION OF THE MELTING BEHAVIOR OF MUSCOVITE SCHISTS

Phase relations during dehydration-melting

The dehydration-melting solidus of MS has a positive dP/dT slope of ~50 bar/°C. It extends from ~750°C at 6 kbar to ~830°C at 10 kbar (Fig. 3). Dehydration-melting of MBS begins at temperatures 15–30°C lower,

along a solidus that is nearly parallel to that of MS (Fig. 3). Between 6 and 10 kbar, dehydration-melting in MS and MBS begins at temperatures 50–80°C higher than in the end-member assemblage muscovite + albite + quartz [compare Petö (1976); shown as P76 in Fig. 3]. Two important differences between the model end-member assemblage studied by Petö (1976) and the natural starting materials that we studied are the Ca-bearing plagioclase compositions (Ab_{82} in MBS and Ab_{86} in MS) of our starting materials, and the presence of Fe, Mg, Ti and F in our muscovite (Table 1). Our experiments show that solid solution in both plagioclase and muscovite extends the thermal stability of the assemblage plagioclase + muscovite + quartz relative to that of the equivalent end-member assemblage. All three muscovite-bearing assemblages (MS, MBS and P76 in Fig. 3), however, melt along solidi that have lower dP/dT slopes than biotite dehydration-melting reactions (dashed lines in Fig. 3). This shows that muscovite is more strongly stabilized by increasing pressure than is biotite (Thompson, 1982; Le Breton & Thompson, 1988; Vielzeuf & Montel, 1994). Because this relationship is well known from eclogite-facies rocks (e.g. Mottana *et al.*, 1990; Massonne, 1995), it is additional evidence that the experimentally determined solidi are not kinetic artifacts.

The lower melting temperature of MBS compared with MS reflects their differing muscovite compositions (lower F and Ti contents in MBS; see Table 1) and, perhaps, the presence of tourmaline in MBS. The breakdown of tourmaline lowers the H_2O-saturated leucogranite solidus by 5–20°C (Bénard *et al.*, 1985), but tourmaline can persist to temperatures >800°C in leucogranite magmas (Bénard *et al.*, 1985; Scaillet *et al.*, 1995). In our experiments, B_2O_3 contents of MBS glasses are higher in runs performed at 820°C, 10 kbar than in those performed at 750°C, 6 kbar (see Table 3 and discussion of analytical procedures). Euhedral tourmaline is abundant in the experimental run product of MBS plus 10% added tourmaline, performed at 820°C, 10 kbar (see Fig. 1d). These observations show that tourmaline does not break down in a pseudo-univariant fashion at the vapor-absent solidus. Owing to its persistence above the solidus, tourmaline has a relatively minor effect on solidus temperatures and on near-solidus melt fractions.

The nature of the muscovite dehydration-melting reaction can be inferred from changes in phase abundances that accompany muscovite consumption (Fig. 4a, Table 2). The melting experiments on starting material MS are used for this discussion, because they constitute a more complete data set than those for MBS. Plagioclase and quartz are consumed by the dehydration-melting reaction, but in smaller proportions than muscovite. Potassium feldspar and aluminosilicate are not present in the starting material, but they appear at the solidus and become more abundant with increasing temperature, commonly as intergrowths of euhedral crystals of these two phases plus biotite and glass (Table 2, Figs 1a and c and 4a). Changes in the modal abundance of garnet are uncertain throughout the muscovite reaction interval (Table 2, Fig. 4a), but biotite clearly increases in abundance relative to the starting material, up to the muscovite-out boundary (Table 2, Fig. 4a). Formation of biotite by the incongruent breakdown of muscovite is also confirmed by mass balance, which shows that the mass of (FeO + MgO) dissolved in melt is less than the mass of (FeO + MgO) liberated by muscovite breakdown.

The stoichiometry of the muscovite dehydration-melting reaction is given by the difference between the phase abundances in experimental run products at conditions that just exceed the muscovite-out boundary (e.g. MS experiment at 820°C, 6 kbar, Table 2) and those in the starting material. This difference yields the following results, in mass proportions [mineral abbreviations after Kretz (1983)]:

$$22\text{Ms} + 7\text{Pl} + 8\text{Qtz} \rightarrow 25\text{Melt} + 5\text{Kfs} + 5\text{Sil} + 2\text{Bt}. \quad (1)$$

It should be noted that because this stoichiometry is calculated on the basis of an experimental run product in which all muscovite has been consumed, but in which biotite breakdown has not begun (see below), it is likely to be an accurate representation of the dehydration-melting reaction. This is so regardless of the metastable persistence of muscovite in the melting experiments, because the crystallization experiment shows that melt compositions are not affected by it. In nature, the dehydration-melting reaction could be completed at lower temperature than in the experiments, but the relative proportions of phases consumed and produced should still be approximately the same as those given by reaction (1). Use of mass proportions makes it possible to apply this reaction in a straightforward way to predict the behavior of natural protoliths. For example, reaction (1) shows that, in the absence of externally derived fluids, muscovite is likely to be the phase that limits melt production, because dehydration-melting consumes a mass of muscovite approximately three times greater than those of plagioclase or quartz. Reaction (1) also shows that the maximum amount of melt that can be produced by dehydration-melting is only slightly greater than the mass of muscovite in the protolith (approximately $25/22 = 1{\cdot}14$ times greater).

A muscovite dehydration-melting reaction of the general form of reaction (1) was proposed by Thompson (1982), Le Breton & Thompson (1988), Vielzeuf & Holloway (1988), and Brearley & Rubie (1990). It differs from the one proposed by Patiño Douce & Johnston [1991, reaction (2)], in that biotite is a net product of

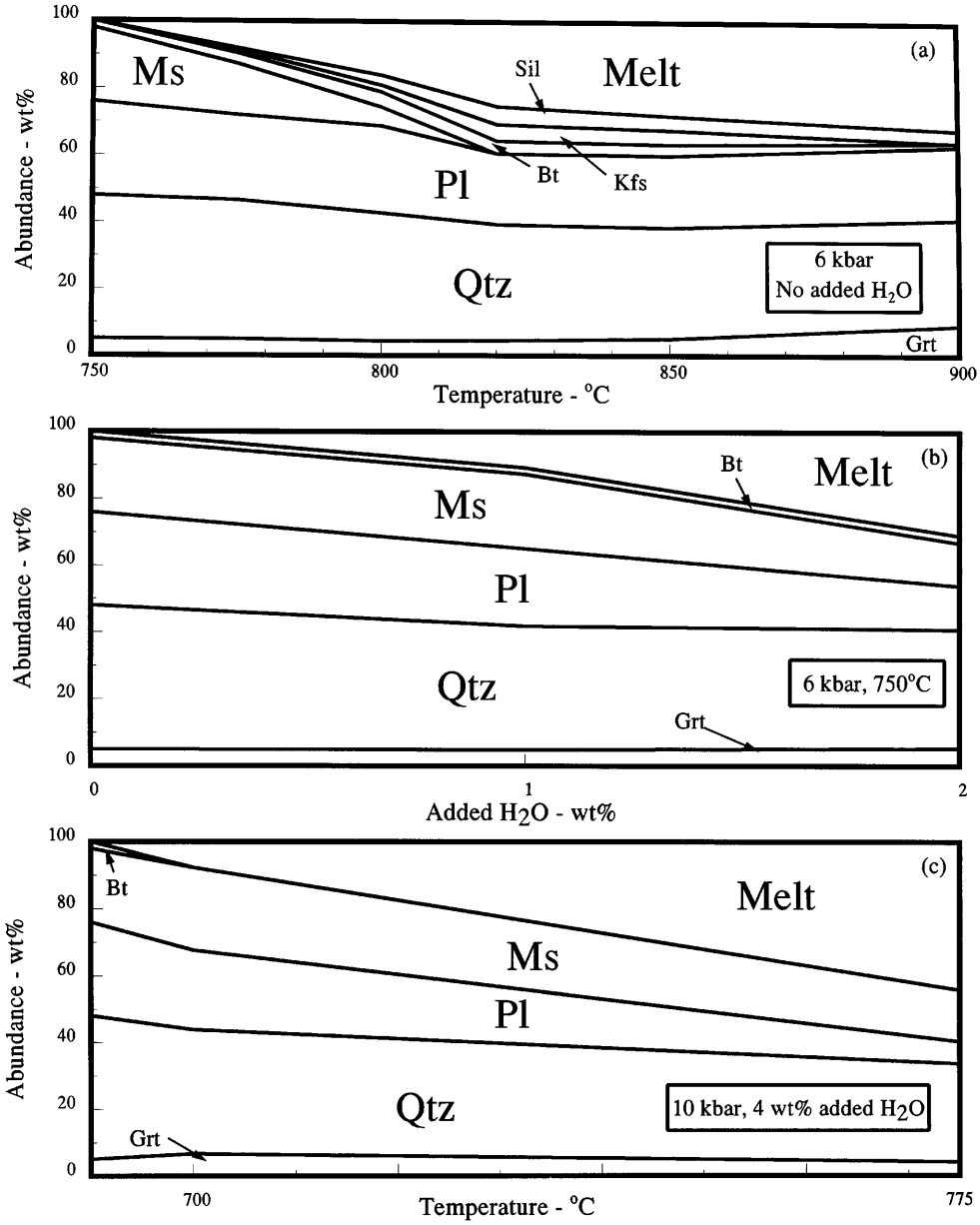

Fig. 4. Phase abundances in selected series of run products with starting material MS [mineral abbreviations after Kretz (1983)]. (a) Dehydration-melting at 6 kbar. (b) Melting at 6 kbar, 750°C with varying amounts of added H_2O. (c) Melting at 10 kbar with 4 wt % added H_2O, as a function of temperature. (Note difference in the ratio of plagioclase to muscovite consumed by the melting reactions with and without added H_2O, and the increasing consumption of plagioclase with increasing pressure.) Owing to metastable persistence of muscovite in the experiments (especially in dehydration-melting ones), the melting reactions in nature could be completed at temperatures lower than those shown in the figure. The relative proportions of phases consumed and produced, however, would nevertheless be approximately the same as those shown here (see text).

the reaction. Patiño Douce & Johnston (1991) argued that biotite and muscovite were both reactants during initial dehydration-melting of metapelites (their fig. 11a, invariant point I_1). Such a reaction requires that the initial melt be richer in Mg and Fe than muscovite. The experiments that we report here, however, show that the initial melt is less rich in Mg and Fe than muscovite. Muscovite and biotite must therefore be in a peritectic relationship during dehydration-melting, as has been argued by Thompson (1982), Le Breton & Thompson (1988), Vielzeuf & Holloway (1988), and Brearley & Rubie (1990), and confirmed by reaction (1).

Reaction (1) and Fig. 4a show that the role of garnet during muscovite dehydration-melting is that of an inert phase, i.e. it neither crystallizes nor dissolves. This is further confirmed by its textural characteristics and by garnet compositions in experimental run products that do not depart significantly from those in the starting materials (Fig. 2).

Melting at temperatures higher than those of the muscovite-out boundary is controlled by the dissolution of potassium feldspar and the incongruent breakdown of biotite, which produces garnet. This change in the melting reaction is reflected in the strong increase in garnet abundance and in the change in its textural characteristics and composition in the experiments at 900°C, 6 and 10 kbar (Table 2, Figs 2 and 4a). Changes in the modal abundances of aluminosilicate and plagioclase suggest that the Al_2O_3 required for garnet crystallization is predominantly supplied by the consumption of sillimanite at 6 kbar, and that reaction of anorthite to grossular becomes an important source of Al_2O_3 at 10 kbar (see also Patiño Douce & Beard (1995, 1996)].

Effects of added H_2O on melting relations

The H_2O-fluxed melting reaction of MS differs from its dehydration-melting reaction (Fig. 4). During dehydration-melting, H_2O is supplied by incongruent breakdown of muscovite, which is therefore consumed in greater proportion than plagioclase [Fig. 4a, reaction (1)]. In contrast, H_2O-fluxed melting consumes plagioclase in greater proportion than muscovite (Table 2, Fig. 4b), because increasing H_2O activity depresses the plagioclase + quartz solidus more strongly than it depresses the stability of micas (see also Conrad *et al.* (1988) and Patiño Douce (1996)]. For example, the difference in phase abundances between the experiment at 6 kbar, 750°C with 2 wt % added H_2O and the starting material suggests the following stoichiometry (in mass proportions) for the melting reaction at these P–T–$X(H_2O)$ conditions:

$$9Ms + 15Pl + 7Qtz + xH_2O \rightarrow 31\ Melt. \quad (2)$$

The H_2O in this reaction represents the H_2O added to the capsule, which is dissolved in the melt at the end of the experiment. Its stoichiometric coefficient remains undetermined because the phase compositions in Table 2 are calculated on an H_2O-free basis. The H_2O-fluxed melting reaction (2) contrasts sharply with the dehydration-melting reaction (1). In the case of H_2O-fluxing the melting behavior is eutectic-like, with plagioclase accounting for approximately half of the reacting mass of rock (compare also Fig. 4a and Fig. 4b). Muscovite in this case dissolves congruently in the melt, so that the K-feldspar + sillimanite + biotite intergrowths characteristic of dehydration-melting are not formed during H_2O-fluxed melting (compare Fig. 1a and Fig. 1b).

The relative proportions of plagioclase and muscovite consumed during H_2O-fluxed melting depend on temperature and pressure. More muscovite reacts out with increasing temperature, as shown by a comparison of the experiments with 2 wt % added H_2O at $P = 6$ kbar and $T = 750$ and 775°C (Table 2). Plagioclase consumption is favored by melting at a lower temperature and higher pressure (Table 2, also compare Fig. 4b and Fig. 4c). An extreme example of how the roles of muscovite and plagioclase change with pressure and temperature is given by the experiment at 10 kbar, 700°C with 4 wt % added H_2O, for which the inferred stoichiometry (in mass proportions) is

$$2Bt + 4Pl + 6Qtz + xH_2O \rightarrow 8Melt + 2Grt + 3Ms. \quad (3)$$

In this experimental run, muscovite is a product of the melting reaction, compared with a reactant in experimental runs at lower pressures and higher temperatures, and biotite becomes a reactant [compare reaction (2)]. This unusual melting reaction can be understood better by breaking it up into two separate reactions that take place concurrently. These reactions are a plagioclase + quartz + H_2O melting reaction, and the following reaction among solid phases:

$$3An + Bt \rightarrow Grs + (Alm + Prp) + Ms. \quad (4)$$

The assemblage garnet + muscovite is on the low-T, high-P side of reaction (4). Therefore, reaction (3) suggests that melting in the 700°C, 10 kbar experiment took place at lower T and/or higher P than the natural equilibration conditions of the starting material MS (Fig. 3). Given the absence of migmatitic features in MS, this result is important because it argues against the pervasive presence of free H_2O (which would have induced melting) in the kyanite-zone metapelites near the base of the High Himalayan Crystalline Sequence.

Melt compositions

All melts generated in our experiments contain >73 wt % SiO_2 (on an H_2O-free basis) and are strongly peraluminous, with molar $Al_2O_3/(CaO + Na_2O + K_2O)$ (A/CNK) generally >1·1 (Table 3). Only melts generated in two experiments on MS with 4 wt % added H_2O (at 10 kbar, 700 and 775°C) have A/CNK < 1·1, owing to the subordinate participation of muscovite in the melting reaction at these conditions [e.g. reaction (3)]. In the products of dehydration-melting experiments, melts of the MBS starting material are richer in CaO than are melts of MS (Table 3, Figs 5 and 6). This probably reflects the more anorthitic plagioclase of the MBS starting material (Table 1).

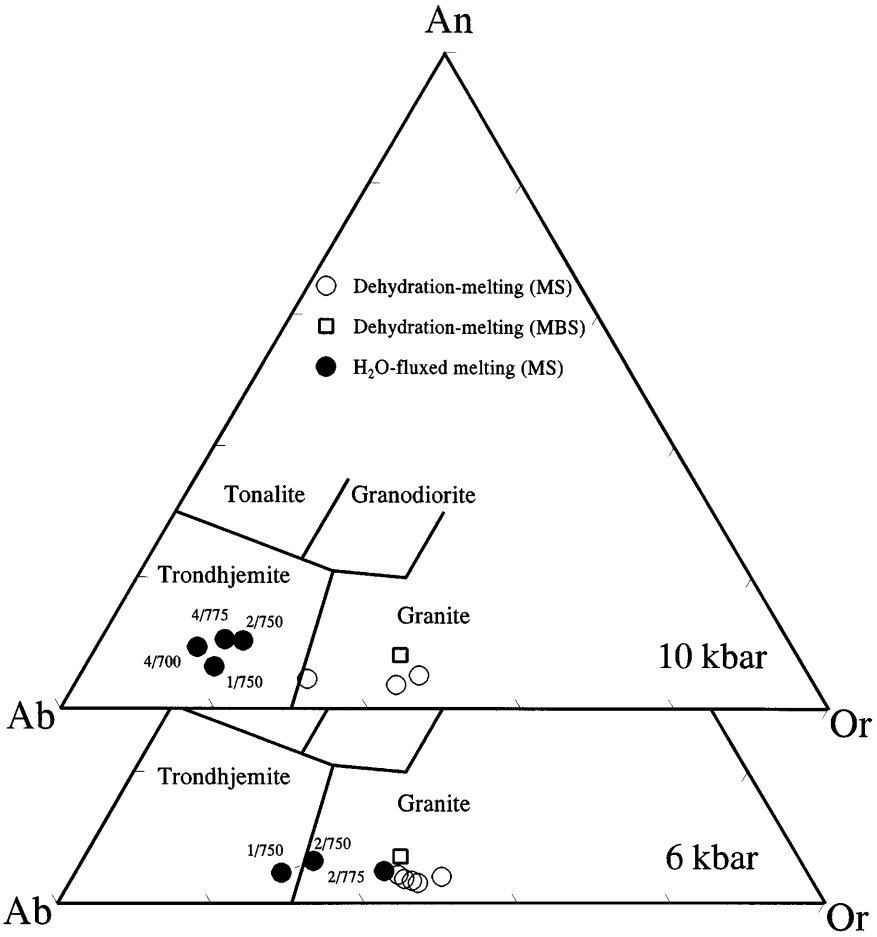

Fig. 5. Normative albite–anorthite–orthoclase contents of experimental glasses, compared with the classification for silicic rocks proposed by Barker (1979). Numbers next to symbols for H_2O-fluxed melts are wt % added H_2O/temperature (in °C).

All melts from both starting materials are leucocratic, with (FeO + MgO + TiO_2) ranging from 0·8 to 1·6 wt % (Table 3). Several arguments indicate that these leucocratic melt compositions closely approach those that would form in nature and are not caused by sluggish reaction kinetics in the experiments. In the first place, glass in the crystallization experiment on MBS at T = 820°C, P = 10 kbar contains virtually the same concentrations of FeO, MgO and TiO_2 as that in the melting experiment at the same conditions (Table 3). In the second place, biotite crystallizes in the dehydration-melting experiments, showing that the melt cannot dissolve all of the FeO + MgO + TiO_2 liberated by muscovite breakdown.

The most notable changes in melt compositions with pressure and H_2O content are in their relative proportions of normative albite, anorthite and orthoclase (Fig. 5). Products of dehydration-melting of both starting materials are granitic in composition, a feature that reflects the fundamental role of muscovite breakdown. However, the Na_2O/K_2O ratios of low melt fractions ($\leq$8 wt %) produced close to the MS dehydration-melting solidus (Table 2) increase from 0·83 at 775°C and 6 kbar, to 0·98 at 800°C and 8 kbar, and 1·45 at 835°C and 10 kbar (Table 3). This trend arises from the inverse correlation between pressure and plagioclase stability, which causes the plagioclase:muscovite ratio in the melting reaction to increase with pressure [see also Patiño Douce & Beard (1995, 1996)]. Increased melting of plagioclase with pressure is also reflected in higher Al_2O_3 and CaO contents of 10 kbar melts than 6 kbar melts (Fig. 6).

Near-solidus melts produced with small amounts of added H_2O are of trondhjemitic composition (Fig. 5, Table 3). This results from the decrease in the temperature of the plagioclase + quartz solidus with increasing H_2O activity, which triggers melting within the muscovite stability field (Fig. 4b and c). The shift towards

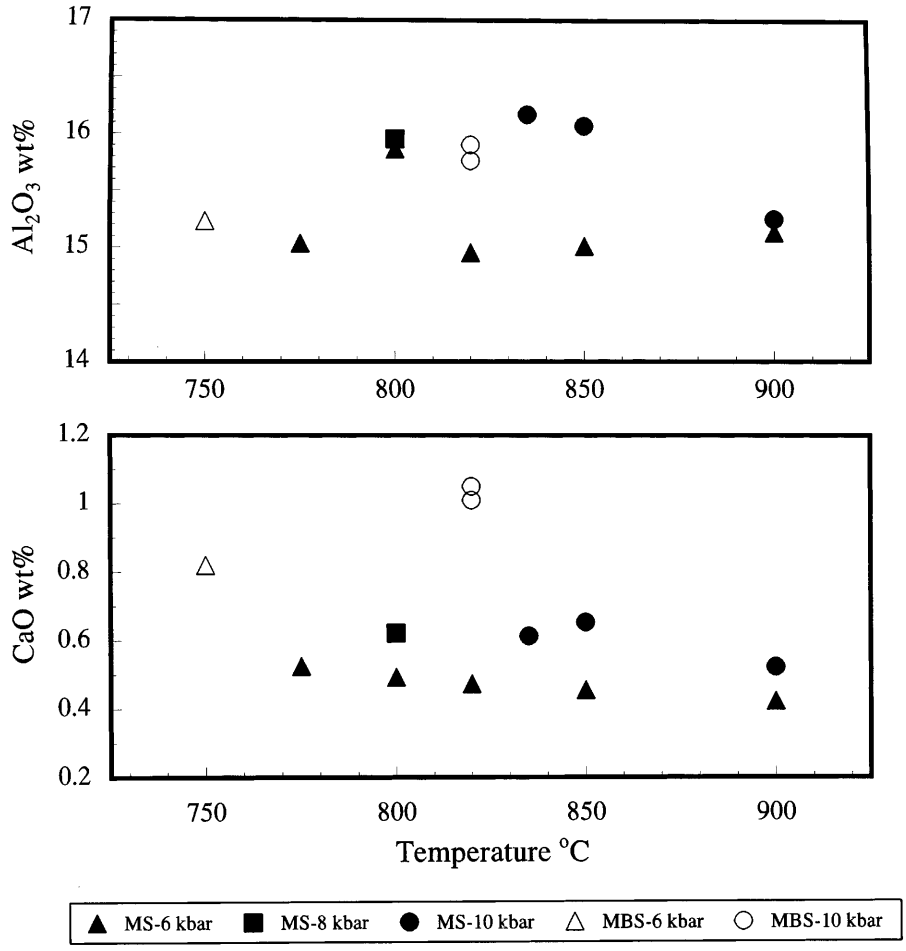

Fig. 6. Al_2O_3 and CaO contents in experimental glasses. In each bulk composition, contents of both oxides are generally higher at 10 kbar than at 6 kbar, reflecting breakdown of plagioclase with increasing pressure.

trondhjemitic compositions is stronger at 10 kbar than at 6 kbar, because increasing pressure expands the stability field of muscovite but reduces that of plagioclase. The most sodic of all the melts was that generated at 10 kbar and 700°C with 4 wt % added H_2O. However, melts produced at 10 kbar remain trondhjemitic at 750°C with up to at least 2 wt % of H_2O added to the starting material, and at 775°C with up to at least 4 wt % added H_2O (Fig. 5). Melts generated at 6 kbar and 750°C with 1 wt % added H_2O are also trondhjemitic. However, with increasing H_2O content and/or temperature at 6 kbar, enough muscovite reacts out to drive the melts towards granitic compositions (Fig. 5).

GEOLOGICAL IMPLICATIONS

Leucogranite generation in the Himalaya

The pressure, temperature and H_2O content under which leucogranite magmas formed in the Himalaya can be estimated from the results of our metapelite melting experiments complemented by those of earlier studies of the phase relations of Himalayan leucogranites (Scaillet *et al.*, 1995). Himalayan leucogranite bodies are of two types: (1) two-mica leucogranites, which commonly display a subsolidus deformational foliation; and (2) muscovite + tourmaline-bearing leucogranites, which are typically undeformed and show cross-cutting relations that suggest that they post-date the two-mica leucogranites. The two-mica granites show lower Rb/Sr ratios, and higher TiO_2, CaO, Ba, and LREE contents relative to the muscovite + tourmaline-bearing leucogranites (Guillot & Le Fort, 1995; Ayres *et al.*, 1997). There are at least three mechanisms that can account for the two types of leucogranites: (1) muscovite + tourmaline-bearing leucogranites can be formed by fractional crystallization of two-mica leucogranites (Scaillet *et al.*, 1990); (2) they may represent different melt fractions of the same source (Harris *et al.*, 1993), with the

two-mica leucogranites representing somewhat hotter melts [see also Scaillet *et al.* (1995)]; or (3) they may represent melts of different metasedimentary protoliths (Guillot & Le Fort, 1995). The three genetic models are not exclusive of each other, and all may be true in specific cases. The major element compositions of both types of leucogranites are similar enough, however, that we can use them both in a comparison with experimental results.

All but one of the analyses of muscovite + tourmaline-bearing and two-mica leucogranites from the Langtang region of the Himalaya (Inger & Harris, 1993) overlap with melt compositions produced by our dehydration-melting experiments at 6–10 kbar (Fig. 7). In contrast, a single two-mica granitoid from this region (SKG9) plots in the trondhjemite field and resembles the H_2O-fluxed melts that we produced at 10 kbar. This trondhjemite may be a rare example of melting related to early H_2O-fluxing of a metapelitic source rock. Except for this rock, the muscovite + tourmaline-bearing leucogranites and the two-mica leucogranites of the Langtang region could have been produced by dehydration-melting in the absence of fluid infiltration (see Harris *et al.*, 1993). Granitic melts similar to the Himalayan leucogranites could also have been formed by H_2O-fluxing, if H_2O infiltration and/or temperature were high enough to cause abundant muscovite breakdown (Figs 5 and 7). However, the residues formed by H_2O-fluxed melting of muscovite schist contain significantly less plagioclase than those formed by dehydration-melting. Melts formed by dehydration-melting are therefore likely to have higher Rb/Sr ratios and lower Ba contents than those formed by H_2O fluxing. For example, for typical pelitic compositions, melts with Rb/Sr ratios >5 result from dehydration-melting, whereas Rb/Sr ratios in melts formed by H_2O-fluxing are generally <2 (Harris *et al.*, 1993, fig. 3). Anatectic melts with low Rb/Sr have been identified only rarely in the Himalaya.

With the notable exception of trondhjemite SKG9, the (FeO + MgO + TiO_2) and CaO contents of Himalayan leucogranites overlap with those of melts produced by experimental dehydration-melting of MS and MBS at temperatures of 750–900°C (Fig. 8). This agreement suggests that most of these leucogranites are nearly pure liquid compositions. Two samples (a two-mica leucogranite and a muscovite + tourmaline-bearing leucogranite, Fig. 8) are slightly more mafic than the experimentally produced melts. These rocks may contain some cumulate material of either restitic or magmatic origin.

Scaillet *et al.* (1995) studied the phase relations of two natural Himalayan leucogranites. They concluded that most of these granitic bodies were probably emplaced as essentially pure liquids containing between 5 and 7·5 wt % H_2O, and at temperatures between 700 and 750°C. Glass compositions in all of our lowest temperature (T = 750–835°C, see Tables 3 and 6) dehydration-melting experiments with MS and MBS at 6, 8 and 10 kbar are averaged and compared with the compositions of the starting materials used by Scaillet *et al.* (1995) in Table 6. The average experimental glass is very similar to the Himalayan leucogranites studied by Scaillet *et al.* (1995), emphasizing that the latter are likely to represent almost pure liquid compositions. Moreover, the H_2O content of our average melt composition, estimated by difference from 100 wt %, is of the order of 5·6 wt %, which is in excellent agreement with the estimate by Scaillet and co-workers of the initial H_2O content of the Himalayan leucogranite magmas.

The formation temperature of the Himalayan leucogranite magmas can be estimated by comparing our experimental results with the thermal evolution of the Himalayan orogen. Harris & Massey (1994) proposed that rocks that were buried deeply in the orogenic belt underwent an uplift history that was fast enough to cause adiabatic decompression. The proposed decompression path for peak thermal conditions is shown in Fig. 3 (after Harris & Massey, 1994). This path intersects the dehydration-melting solidi of MS and MBS at 750°C and 6–8 kbar. Initial temperatures of the order of 750°C may thus be possible for the generation of Himalayan leucogranite magmas under fluid-absent conditions, provided that melting occurred shallower than ~30 km, or $P < 8$ kbar (Fig. 3). Melting at greater depths would have been possible only if the metapelite source rocks were infiltrated by aqueous fluids. However, H_2O-fluxed melting at $P > 8$ kbar generates melts of trondhjemitic composition (Fig. 5), which are clearly different from the Himalayan leucogranites (Fig. 7).

Independent studies of crystallization of Himalayan leucogranite magmas (Scaillet *et al.*, 1995) and of melting of their likely protoliths (this study) yield consistent estimates for the initial temperatures (~750°C) and H_2O contents (~5·6 wt %) of the magmas. Generation of leucogranite magmas at these conditions must have taken place at depths of less than ~30 km, during fast adiabatic decompression.

Anatexis may thus have affected only the upper half of the tectonically thickened Himalayan crust.

K-rich metasediments as sources of trondhjemite melts

Trondhjemite melts can be generated from low-temperature (700–750°C) H_2O-fluxed melting of K-rich metasedimentary source rocks [Table 3, Figs 5 and 7; see also Conrad *et al.* (1988) and Patiño Douce (1996)].

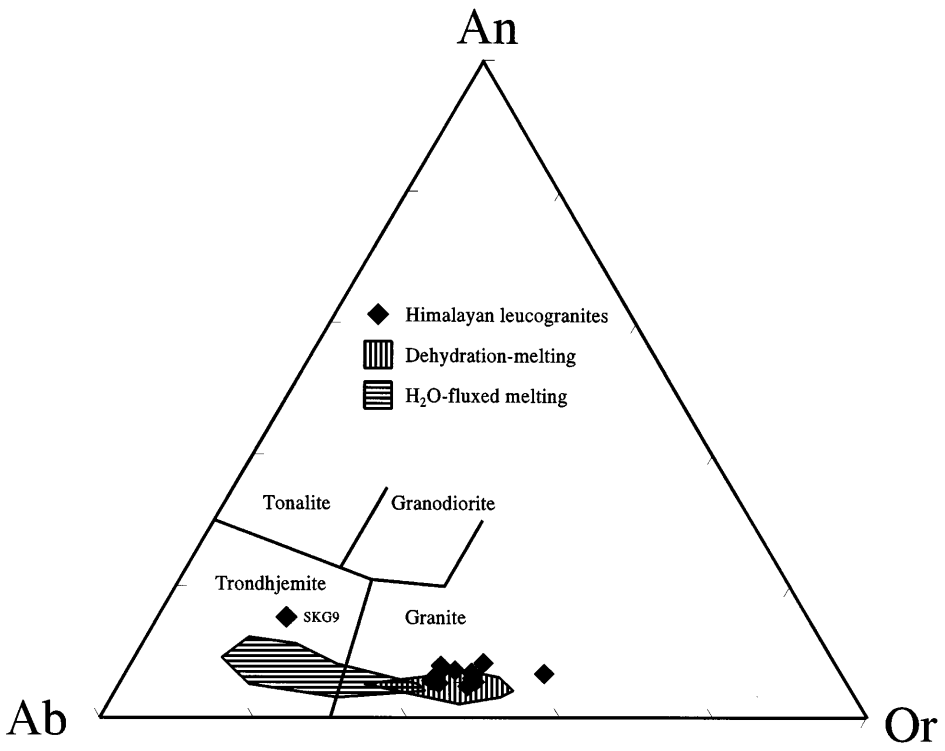

Fig. 7. Compositional ranges of experimentally generated melts (patterned areas) compared with Himalayan leucogranites (Inger & Harris, 1993). The compositions of two-mica and muscovite–tourmaline-bearing leucogranites overlap, so they are plotted with a single symbol. SKG9 is a clearly different two-mica trondhjemite.

This requires a combination of little influx of H_2O, low enough temperature and high enough pressure to preserve muscovite in the residue (Table 2, Fig. 4). Residues rich in mica + quartz and depleted in plagioclase, formed by H_2O-fluxed melting of metasedimentary rocks [compare Fig. 4b and Fig. 4c, reaction (2)], are still fertile magma sources. They can generate significant volumes of K-rich granitic melts by dehydration-melting at temperatures >850°C (Patiño Douce & Johnston, 1991).

Migmatites with trondhjemitic leucosomes and mica-rich melanosomes (e.g. Whitney & Irving, 1994) are a possible outcome of H_2O-fluxed melting of metapelitic rocks. Such migmatites could represent the earliest appearance of melt during prograde metamorphism of a thickening orogenic belt. This early, deep and relatively 'cold' migmatite environment is a very different setting from that in which leucogranite magmas form. The latter are the products of fast transport of deep-seated rocks to shallow crustal levels, caused almost certainly by tectonic collapse late in the orogenic cycle. At least in some cases, therefore, migmatization and granite magma genesis are processes that are likely to be separated in space and time.

Dehydration-melting of muscovite schists and biotite schists compared

The dP/dT slope of the muscovite dehydration-melting reaction is considerably less than that of the biotite dehydration-melting reaction. Because of this difference, muscovite schist can be either less or more refractory than biotite schist, depending on the depth at which melting conditions are attained (see also Le Breton & Thompson, 1988). Figure 3 compares the dehydration-melting solidi of Himalayan metapelites with those of three biotite schists of differing *mg*-number [Patiño Douce & Beard (1995), *mg*-number 55; Vielzeuf & Montel (1994), *mg*-number 44; and Patiño Douce & Beard (1996), *mg*-number 23], and with those of the end-member assemblages phlogopite + quartz (Vielzeuf & Clemens, 1992) and muscovite + albite + quartz (Petö, 1976). At pressures lower than 9 kbar, dehydration-melting of muscovite schist always takes place at lower temperature than that of biotite schist. At such pressures, muscovite schist generates leucogranite melts at 750–800°C, but interlayered biotite schist would remain unmolten (Fig. 3). As pressure increases the muscovite and biotite dehydration-melting solidi cross over, so that, in the absence

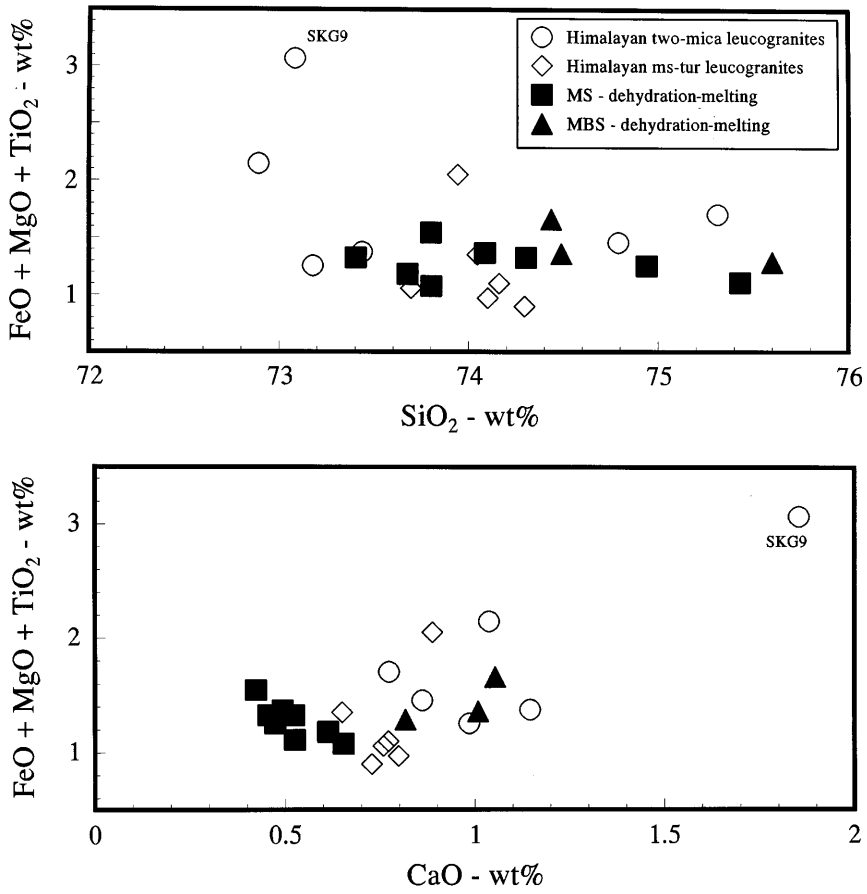

Fig. 8. Contents of SiO_2, CaO and (FeO + MgO + TiO_2) in glasses in the experimental run product, compared with Himalayan leucogranites (Inger & Harris, 1993). One two-mica granite and one muscovite–tourmaline-bearing granite have somewhat higher ferromagnesian contents than the experimental melts. Trondhjemite SKG9 is again clearly different. Most of the Himalayan leucogranites, however, may represent virtually pure melts formed by dehydration-melting of muscovite schist.

of infiltration of aqueous fluids, muscovite schist will be more refractory than biotite schist. The actual pressure of the crossover depends on the *mg*-number of the biotite, the Ti and F contents of both biotite and muscovite, and the plagioclase composition of the source rock. The crossover pressure could be as low as 9 kbar (see Fig. 3), which suggests that in deep levels of tectonically thickened orogens (>35 km deep), muscovite schist could be an important H_2O reservoir, even if biotite schist underwent anatexis.

Also because of the different slopes of their dehydration-melting solidi, decompression-melting is likely to be a more significant process in muscovite schist than in biotite schist. Adiabatic decompression paths (such as the one shown in Fig. 3) intersect the relatively flat dehydration-melting solidus of muscovite schist, triggering anatexis at relatively shallow depths. Leucogranite intrusive bodies in the Himalaya, and probably in other orogenic belts as well, are almost certainly the outcome of relatively shallow decompression-melting of muscovite schists. In contrast, the steep solidi for dehydration-melting of biotite schists are almost parallel to adiabatic decompression paths. This means that, if biotite schists remain unmolten when buried deeply in an orogenic belt, they are also unlikely to melt during the ensuing decompression.

ACKNOWLEDGEMENTS

We thank Bruno Scaillet, Bernard Evans and Howard Day for their helpful and constructive reviews of the manuscript, and Sorena Sorensen for her editorial help. The experimental work was supported by NSF Grant EAR-9316304 to A.E.P.D. The microprobe at the University of Georgia was acquired with NSF Grant EAR-8816748 and a matching grant from the University of Georgia Research Foundation. We thank Linda Kirstein and Alan Whittington for geochemical analyses of source rocks, and Mike Ayres for providing sample PAN-3.

Table 6: Comparison with Himalayan leucogranites

Oxide (wt %)	Experimental glasses[1]	Two-mica leucogranite[2]	Ms–tur leucogranite[3]
SiO_2	74·66	73·59	73·88
Al_2O_3	15·63	15·44	15·77
TiO_2	0·14	0·13	0·06
FeO*[4]	0·93	0·90	0·75
MgO	0·27	0·20	0·14
MnO	0·04	0·01	0·01
CaO	0·73	0·86	0·58
Na_2O	3·75	3·88	4·62
K_2O	3·87	5·00	4·19
Total[5]	94·40	—	—

[1]Average of the glass compositions in the following five dehydration-melting experimental run products (data from Table 3): MS at 6 kbar, 775°C; MS at 8 kbar, 800°C; MS at 10 kbar, 835°C; MBS at 6 kbar, 750°C; and MBS at 10 kbar, 820°C (melting experiment only). These are the lowest temperature experimental run products for each starting material and at each pressure investigated in which glass was identified and/or could be reliably analyzed. The average was then recalculated to 100 wt % volatile-free.
[2]Two-mica leucogranite starting material of Scaillet *et al.* (1995), sample DK89. Recalculated to 100 wt % volatile-free.
[3]Muscovite–tourmaline-bearing leucogranite starting material of Scaillet *et al.* (1995), sample GB4. Recalculated to 100 wt % volatile-free.
[4]Total Fe recalculated as FeO.
[5]Average of the microprobe analytical totals for the five experimental glass compositions. Difference to 100 wt % yields an estimated H_2O content of 5·6 wt % (see text for discussion).

N.H. acknowledges the Royal Society for research grants supporting Himalayan field-work.

REFERENCES

Ayres, M., Harris, N. & Vance, D. (1997). Possible constraints on anatectic melt residence times from accessory mineral dissolution rates: an example from Himalayan leucogranites. *Mineralogical Magazine* **61,** 29–36.

Barker, F. (1979). Trondhjemite: definition, environment and hypotheses of origin. In: Barker, F. (ed.) *Trondhjemites, Dacites, and Related Rocks. Developments in Petrology, 6.* Amsterdam: Elsevier, pp. 1–12.

Bénard, F., Moutou, P. & Pichavant, M. (1985). Phase relations of tourmaline leucogranites and the significance of tourmaline in silicic magmas. *Journal of Geology* **93,** 271–291.

Berman, R. G. (1988). Internally-consistent thermodynamic data for stoichiometric minerals in the system Na_2O–K_2O–CaO–MgO–FeO–Fe_2O_3–Al_2O_3–SiO_2–TiO_2–H_2O–CO_2. *Journal of Petrology* **29,** 445–522.

Berman, R. G. (1990). Mixing properties of Ca–Mg–Fe–Mn garnets. *American Mineralogist* **75,** 328–344.

Brearley, A. J. & Rubie, D. C. (1990). Effects of H_2O on the disequilibrium breakdown of muscovite + quartz. *Journal of Petrology* **31,** 925–956.

Carrington, D. P. & Harley, S. L. (1995). Partial melting and phase relations in high-grade metapelites: an experimental petrogenetic grid in the KFMASH system. *Contributions to Mineralogy and Petrology* **120,** 270–291.

Castelli, D. & Lombardo, B. (1988). The Gophu La and Western Lunana granites: Miocene muscovite leucogranites of the Bhutan Himalaya. *Lithos* **21,** 211–225.

Clemens, J. D. & Vielzeuf, D. (1987). Constraints on melting and magma production in the crust. *Earth and Planetary Science Letters* **86,** 287–306.

Conrad, W. K., Nicholls, I. A. & Wall, V. J. (1988). Water-saturated and -undersaturated melting of metaluminous and peraluminous crustal compositions at 10 kb: evidence for the origin of silicic magmas in the Taupo Volcanic Zone, New Zealand, and other occurrences. *Journal of Petrology* **29,** 765–803.

Dooley, D. F. & Patiño Douce, A. E. (1996). Vapor-absent melting of F- and Ti-rich phlogopite + quartz; effects on phlogopite stability and melt compositions. *American Mineralogist* **81,** 202–212.

France-Lanord, C. & Le Fort, P. (1988). Crustal melting and granite genesis during the Himalayan collision orogenesis. *Transactions of the Royal Society of Edinburgh: Earth Sciences* **79,** 183–195.

France-Lanord, C., Sheppard, S. M. F. & Le Fort, P. (1988). Hydrogen and oxygen isotope variations in the High Himalaya peraluminous Manaslu leucogranite: evidence for heterogeneous sedimentary source. *Geochimica et Cosmochimica Acta* **52,** 513–526.

Fuhrman, M. L. & Lindsley, D. H. (1988). Ternary-feldspar modeling and thermometry. *American Mineralogist* **73,** 201–215.

Gardien, V., Thompson, A. B., Grujic, D. & Ulmer, P. (1995). Experimental melting of biotite + plagioclase + quartz ± muscovite assemblages and implications for crustal melting. *Journal of Geophysical Research* **100,** 15581–15591.

Guillot, S. & Le Fort, P. (1995). Geochemical constraints on the bimodal origin of High Himalayan leucogranites. *Lithos* **35,** 221–234.

Harris, N. & Ayres, M. (1997). The implications of Sr-isotope disequilibrium for rates of prograde metamorphism and melt extraction in anatectic terrains. *Geological Society, London, Special Publication* (in press).

Harris, N. & Massey, J. (1994). Decompression and anatexis of the Himalayan metapelites. *Tectonics* **13,** 1537–1546.

Harris, N., Inger, S. & Massey, J. (1993). The role of fluids in the formation of High Himalayan leucogranites. In: Treloar, P. J. & Searle, M. P. (eds) *Himalayan Tectonics. Geological Society, London, Special Publication* **74,** 391–400.

Harris, N., Ayres, M. & Massey, J. (1995). Geochemistry of granitic melts produced during the incongruent melting of muscovite: implications for the extraction of Himalayan leucogranite magmas. *Journal of Geophysical Research* **100,** 15767–15777.

Holtz, F. & Johannes, W. (1991). Genesis of peraluminous granites I. Experimental investigation of melt compositions at 3 and 5 kb and various H_2O activities. *Journal of Petrology* **32,** 935–958.

Huang, W. L. & Wyllie, P. J. (1973). Melting relations of muscovite granite to 35 kbar as a model for fusion of metamorphosed subducted oceanic sediments. *Contributions to Mineralogy and Petrology* **42,** 1–14.

Huang, W. L. & Wyllie, P. J. (1981). Phase relationships of S-type granites with H_2O to 35 kbar: muscovite granite from Harney Peak, South Dakota. *Journal of Geophysical Research* **86,** 10515–10529.

Inger, S. & Harris, N. (1992). Tectonothermal evolution of the High Himalayan Crystalline Sequence, Langtang Valley, northern Nepal. *Journal of Metamorphic Geology* **10,** 439–452.

Inger, S. & Harris, N. (1993). Geochemical constraints on leucogranite magmatism in the Langtang Valley, Nepal Himalaya. *Journal of Petrology* **34,** 345–368.

Kretz, R. (1983). Symbols for rock-forming minerals. *American Mineralogist* **68,** 277–279.

Le Breton, N. & Thompson, A. B. (1988). Fluid-absent (dehydration) melting of biotite in metapelites in the early stages of crustal anatexis. *Contributions to Mineralogy and Petrology* **99,** 226–237.

Le Fort, P. (1981). Manaslu leucogranite: a collision signature of the Himalaya, a model for its genesis and emplacement. *Journal of Geophysical Research* **86,** 10545–10568.

Le Fort, P. (1988). Granites in the tectonic evolution of the Himalaya, Karakorum and southern Tibet. *Philosophical Transactions of the Royal Society of London, Series A* **326,** 281–299.

Le Fort, P., Cuney, M., Deniel, C., France-Lanord, C., Sheppard, S. M. F., Upreti, B. N. & Vidal, P. (1987). Crustal generation of the Himalayan leucogranites. *Tectonophysics* **134,** 39–57.

London, D., Morgan, VI, G. B. & Hervig, R. V. (1989). Vapor-undersaturated experiments with Macusani glass + H_2O at 200 MPa, and the internal differentiation of granitic pegmatites. *Contributions to Mineralogy and Petrology* **102,** 1–17.

Massonne, H.-J. (1995). Experimental and petrogenetic study of UHPM. In: Coleman, R. G. & Wang, X. (eds) *Ultrahigh Pressure Metamorphism*. Cambridge: Cambridge University Press, pp. 33–95.

Mottana, A., Carswell, D. A., Chopin, C. & Oberhänsli, R. (1990). Eclogite facies mineral parageneses. In: Carswell, D. A. (ed.) *Eclogite Facies Rocks*. Glasgow: Blackie, pp. 14–52.

Nabelek, P. I., Russ-Nabelek, C. & Denison, J. R. (1992). The generation and crystallization conditions of the Proterozoic Harney Peak Leucogranite, Black Hills, South Dakota, USA: petrologic and geochemical constraints. *Contributions to Mineralogy and Petrology* **110,** 173–191.

Patiño Douce, A. E. (1995). Experimental generation of hybrid silicic melts by reaction of high-Al basalt with metamorphic rocks. *Journal of Geophysical Research* **100,** 15623–15639.

Patiño Douce, A. E. (1996). Effects of pressure and H_2O content on the compositions of primary crustal melts. *Transactions of the Royal Society of Edinburgh: Earth Sciences* **87,** 11–21.

Patiño Douce, A. E. & Beard, J. S. (1994). Water loss from hydrous melts during fluid-absent piston-cylinder experiments. *American Mineralogist* **79,** 585–588.

Patiño Douce, A. E. & Beard, J. S. (1995). Dehydration-melting of biotite gneiss and quartz amphibolite from 3 to 15 kbar. *Journal of Petrology* **36,** 707–738.

Patiño Douce, A. E. & Beard, J. S. (1996). Effects of P, $f(O_2)$ and Mg/Fe ratio on dehydration-melting of model metagreywackes. *Journal of Petrology* **37,** 999–1024.

Patiño Douce, A. E. & Johnston, A. D. (1991). Phase equilibria and melt productivity in the pelitic system: implications for the origin of peraluminous granitoids and aluminous granulites. *Contributions to Mineralogy and Petrology* **107,** 202–218.

Patiño Douce, A. E., Johnston, A. D. & Rice, J. M. (1993). Octahedral excess mixing properties in biotite: a working model with applications to geobarometry and geothermometry. *American Mineralogist* **78,** 113–131.

Peterson, J. W. & Newton, R. C. (1989). Reversed experiments on biotite–quartz–feldspar melting in the system KMASH: implications for crustal anatexis. *Journal of Geology* **97,** 465–486.

Petö, P. (1976). An experimental investigation of melting relations involving muscovite and paragonite in the silica-saturated portion of the system K_2O–Na_2O–Al_2O_3–SiO_2–H_2O to 15 kb total pressure. *Progress in Experimental Petrology* **3,** 41–45.

Scaillet, B., France-Lanord, C. & Le Fort, P. (1990). Badrinath–Gangotri plutons (Garhwal, India): petrological and geochemical evidence for fractionation processes in a high Himalayan leucogranite. *Journal of Volcanology and Geothermal Research* **44,** 163–188.

Scaillet, B., Pichavant, M. & Roux, J. (1995). Experimental crystallization of leucogranite magmas. *Journal of Petrology* **36,** 663–705.

Searle, M. P. & Fryer, B. J. (1986). Garnet, tourmaline and muscovite-bearing leucogranites of the Higher Himalaya from Zanskar, Kulu, Lahoul and Kashmir. In: Coward, M. P. & Ries, A. C. (eds) *Collision Tectonics. Geological Society, London, Special Publication* **19,** 185–201.

Skjerlie, K. P. & Johnston, A. D. (1993). Fluid-absent melting behavior of an F-rich tonalitic gneiss at mid-crustal pressures: implications for the generation of anorogenic granites. *Journal of Petrology* **34,** 785–815.

Stern, C. R., Kligfield, R., Schelling, D., Virdi, N. S., Futa, K., Peterman, Z. E. & Amini, H. (1989). The Bagirathi leucogranite of the High Himalaya (Garhwal, India); age, petrogenesis and tectonic implications. *Geological Society of America Special Paper* **232,** 33–45.

Storre, B. (1972). Dry melting of muscovite + quartz in the range P_s = 7 kb to P_s = 20 kb. *Contributions to Mineralogy and Petrology* **37,** 87–89.

Storre, B. & Karotke, E. (1972). Experimental data on melting reactions of muscovite + quartz in the system K_2O–Al_2O_3–SiO_2–H_2O to 20 kb water pressure. *Contributions to Mineralogy and Petrology* **36,** 343–345.

Thompson, A. B. (1982). Dehydration melting of pelitic rocks and the generation of H_2O-undersaturated granitic liquids. *American Journal of Science* **282,** 1567–1595.

Thompson, A. B. & Algor, J. R. (1977). Model system for anatexis of pelitic rocks. I. Theory of melting reactions in the system $KAlO_2$–$NaAlO_2$–Al_2O_3–SiO_2–H_2O. *Contributions to Mineralogy and Petrology* **63,** 247–269.

Vielzeuf, D. & Clemens, J. D. (1992). The fluid-absent melting of phlogopite + quartz: experiments and models. *American Mineralogist* **77,** 1206–1222.

Vielzeuf, D. & Holloway, J. R. (1988). Experimental determination of the fluid-absent melting relations in the pelitic system. Consequences for crustal differentiation. *Contributions to Mineralogy and Petrology* **98,** 257–276.

Vielzeuf, D. & Montel, J. M. (1994). Partial melting of metagreywackes. 1. Fluid-absent experiments and phase relationships. *Contributions to Mineralogy and Petrology* **117,** 375–393.

Weidner, J. R. & Martin, R. F. (1987). Phase equilibria of a fluorine-rich leucogranite from the St. Austell pluton, Cornwall. *Geochimica et Cosmochimica Acta* **51,** 1591–1597.

Whitney, D. L. & Irving, J. A. (1994). Origin of K-poor leucosomes in a metasedimentary migmatite complex by ultrametamorphism, syn-metamorphic magmatism, and subsolidus processes. *Lithos* **32,** 173–192.

Williamson, B. J., Shaw, A., Downes, H. & Thirlwall, M. F. (1996). Geochemical constraints on the genesis of Hercynian two-mica leucogranites from the Massif Central, France. *Chemical Geology* **127,** 25–42.